THESIS

MICHIGAN STATE UNIVERSITY LIBRARIES
3 1293 01565 9307

LIBRARY
Michigan State
University

This is to certify that the

dissertation entitled

Optimization of Batch Antisolvent Crystallization

presented by

Satu Marketta Uusi-Penttilä

has been accepted towards fulfillment
of the requirements for

Ph.D. degree in Chemical Engineering

Major professor

Date 5/7/97

MSU is an Affirmative Action/Equal Opportunity Institution

O-12771

PLACE IN RETURN BOX to remove this checkout from your record.
TO AVOID FINES return on or before date due.

DATE DUE	DATE DUE	DATE DUE
MAR 17 2003 04080 3		

MSU is An Affirmative Action/Equal Opportunity Institution
c:\circ\datedue.pm3-p.1

OPTIMIZATION OF BATCH ANTISOLVENT CRYSTALLIZATION

By

Satu Marketta Uusi-Penttilä

A DISSERTATION

Submitted to
Michigan State University
in partial fulfillment of the requirements
for the degree of

DOCTOR OF PHILOSOPHY

Department of Chemical Engineering

1997

ABSTRACT

OPTIMIZATION OF BATCH ANTISOLVENT CRYSTALLIZATION

By

Satu Marketta Uusi-Penttilä

Batch antisolvent crystallization is a commonly used crystallization method in the pharmaceutical industry, which produces very pure crystals with a narrow particle size distribution and high yields. It is also an effective method to crystallize heat sensitive materials, since the crystallization can be achieved at low temperatures.

The objectives of this research were to study the effect of the antisolvent addition rate on various crystallization parameters, including operational parameters and product specification parameters, and to find an operating procedure that produces a desired particle size distribution. The monitoring of the system is done *in situ* using attenuated total reflection Fourier transform infrared (ATR FTIR) spectroscopy.

Since antisolvent crystallization involves two solvents, the polarity behavior of binary systems is addressed first. This involved the introduction of a spectroscopic method to estimate polarities of pure solvents. The same method was applied to binary mixtures. It was shown that even small amounts of antisolvent will cause significant nonideality in the polarity of the system. This should be accounted for in antisolvent crystallization.

The chosen crystallization was l-lysine monohydrochloride purification using water as a solvent and ethanol as an antisolvent. The solubility data for l-lysine monohydrochloride in water, ethanol, and mixtures of water and ethanol were determined. The addition of ethanol decreased the solubility of l-lysine monohydrochloride in water significantly.

The growth kinetics of l-lysine monohydrochloride were estimated from nucleation cell and seeded laboratory scale experiments. These data were used to predict nucleation rates. It was shown that the nucleation rate is very high throughout the crystallization.

The effect of the antisolvent addition rate on bulk supersaturation and particle size was studied. ATR FTIR spectroscopy was used to study the bulk supersaturation. It was shown that the bulk supersaturation was not a function of antisolvent concentration. Sieving showed that the particle size was strongly dependent on the antisolvent addition rate.

This dissertation employed a spectroscopic method for studying solvent polarity behavior. The feasibility of ATR FTIR spectroscopy for monitoring batch antisolvent crystallization was demonstrated. Also, an operating scheme for producing the desired particle size was presented.

ACKNOWLEDGMENTS

I would like to thank my advisor, Dr. Kris Berglund, for his enthusiasm and the relaxed way in which he guided me through my research project. Tack så mycket!

I would like to thank the members of my dissertation committee, Dr. Daina Briedis, Dr. Alec Scranton, and Dr. Gary Blanchard for their interest toward my research.

I acknowledge the financial support from the Fulbright Commission in Finland, Neste Oy Foundation, Helsinki University of Technology, Helsinki University of Technology Foundation, Finnish Cultural Foundation, and U.S. Department of Agriculture.

I would like to thank everybody in the lab. A special thank you goes to Sanjay Yedur who is a true friend. His help in sorting out my research related (and unrelated) disasters is greatly appreciated. Dilum Dunuwila deserves my thanks for guiding me through the mysteries of the infrared spectrometer. I would also like to thank Dr. Hasan Alizadeh for the valuable discussions and practical advice.

I am grateful to Ben and Marie Bohnhorst for proofreading my dissertation and showing me by their own example how to be a good bridge player.

I would like to thank my parents, Sulo and Pirkko Uusi-Penttilä, and my brother, Jyrki, and my sister, Pauliina, for all their support. I would also like to thank my host parents, Frank and Sue Boley. I would have to write another thesis to list all the things they did for me throughout the years.

The biggest thank you goes to my husband Rik who survived this whole ordeal. His support and belief in me were a great help. Our endless walks, talks and bridge sessions were great medication to my stress.

TABLE OF CONTENTS

LIST OF TABLES

LIST OF FIGURES

LIST OF SYMBOLS

A	absorbance, [-]
A_λ	absorbance at λ, [-]
A_{eq}	spherical equivalent area, [mm^2]
A_r	relative absorbance, [-]
a	absorptivity, [dm^3 / g cm]
B_o	nucleation rate, [# / m^3 s]
b	kinetic order of nucleation, [-]
b	pathlength, [cm]
CV	coefficient of variation, [-]
c	concentration, [g/ dm^3]
c_L	concentration of solute in solution, [kg/m^3]
$c_{L,\,eq}$	concentration of solute in solution at equilibrium, [kg/m^3]
Δc	supersaturation, $\Delta c = c_L - c_{L,\,eq}$, [$kg/m^3$]
D	static dielectric constant, [-]
D	difference in second derivative peaks, [-]
d_p	penetration depth, [μm]
$f(D)$	Onsager function, [-]
$f(L)$	Gaussian probability function, [-]
G	growth rate, [μm/min]
g	kinetic order of growth, [-]
I_λ	intensity of the second derivative peak at λ, [-]
j	exponent, [-]
k_g	growth rate constant, [-]
k_N	nucleation rate constant, [-]
k_v	volume shape factor, $k_v = \pi/6$, [-]
L	size, length, [m]
L_i	mean size of a sieve cut i, [μm]
L_{wm}	weight based mean size, [μm]
$L_{16\%}$	particle size at 16% on the cumulative undersize or oversize plot, [μm]
$L_{84\%}$	particle size at 84% on the cumulative undersize or oversize plot, [μm]
l	length of a crystal, [μm]
m_e	mass of ethanol, [g]
m_i	i^{th} moment of the crystal size distribution, [m^{i-3}]
m_L	mass of l-lysine monohydrochloride, [g]
$m_{L,\,eq}$	equilibrium mass of l-lysine monohydrochloride in solution, [g]
m_{Lo}	initial mass of l-lysine monohydrochloride, [g]
m_s	mass of solids, [g]
m_T	suspension density, [kg/m^3]
m_w	mass of water, [kg]
N	number of reflection points in contact with the sample, [-]
n	population density, [# / m^4]
$\hat{n}$	population density based on total volume of the crystallizer, [# / m^4]
n_1	refractive index of the denser material, [-]

n_2	refractive index of the less dense material, [-]
Q_e	volumetric ethanol flowrate, [ml/min]
r	radius of a sphere, characteristic length of a crystal, [μm]
r	correlation coefficient, [-]
S	supersaturation, [-]
T	temperature, [°C]
T	transmittance, [-]
t	time, [min]
V	working volume of crystallizer, [ml]
V_w	volume of water, [ml]
W	mass of crystals in suspension, [kg crystals/kg of solvent]
w	width of a crystal, [μm]
w_i	mass of crystals on sieve i, [g]
w_{llmhc}	weight-% of l-lysine monohydrochloride, [w-%]
η_s	refractive index of sample, [-]
η_c	refractive index of ATR crystal, [-]
θ	incident angle of infrared radiation, [-]
$\lambda_{absorption}$	absorption wavelength, [nm]
λ_c	wavelength in the ATR crystal, [nm]
$\lambda_{emission}$	emission wavelength, [nm]
ρ_c	density of l-lysine monohydrochloride, [g/ml]
ρ_e	density of ethanol, [g/ml]
ρ_w	density of water, [g/ml]
σ	standard deviation of the particle size, [μm]
σ	relative bulk supersaturation, [-]
$\varphi(D)$	Debye function, [-]

Chapter 1

INTRODUCTION

1.1 Crystallization from solution

A wide variety of products in chemical, food, and pharmaceutical industries are manufactured by crystallization from solution. Crystallization can be used to separate or purify a product or an intermediate, and to obtain a solid product with a desired particle size distribution and crystal habit. In many applications the product specifications are very strict. In spite of that the control of crystallizers is still rare, and for most industrial crystallizations a trial-and-error approach is used to meet the product specifications.

Crystallization from solution is especially useful in the pharmaceutical industry where almost all the products are crystallized or precipitated at least once during the manufacturing. Furthermore, at room temperature, the solid state is the most stable form of the majority of pharmaceutical products used today [43]. Crystallization also determines the particle properties of the product that can have a major influence on the pharmaceutical characteristics of the drug [43]. Properties, like bulk density, particle size distribution, surface area, crystal form, and crystal shape, all have an effect on the bioavailability of the active component; and consequently, they directly affect the dosage of the drug. The particle size distribution can also be critical in downstream processing, including steps like tableting, filtration and pumping.

Crystallization is, however, a complicated operation. To achieve a desired crystal size distribution the driving force of crystallization, i.e. supersaturation, has to be controlled. Supersaturation control is very difficult since the factors that influence the crystal size distribution also have feedback effects [44], [59], as demonstrated in Figure 1.1. Therefore, the mass balance, population balance, and growth and nucleation kinetic equations have to be solved simultaneously to obtain the crystal size distribution.

1.2 Research objectives

The goal of this research is to develop an operating strategy for a batch antisolvent crystallization system to obtain a desired crystal size distribution. Attenuated total reflection Fourier transform infrared spectroscopy will be used to monitor the liquid phase *in situ* during the crystallization. The infrared data will be used to study the effect of antisolvent addition rate on various parameters. The model system will be l-lysine monohydrochloride purification from aqueous solution using ethanol as the antisolvent. This study will provide better control of product quality and reduce batch-to-batch variations in process performance.

1.3 Batch crystallization

1.3.1 Background

The bulk production of pharmaceuticals handles much smaller quantities of product than most other chemical industries, such as inorganic chemicals or fertilizers. Therefore, pharmaceutical production is usually done in batch mode. The main advantage of batch crystallization over continuous crystallization is the simpler equipment. The same crystallizer can be used for a

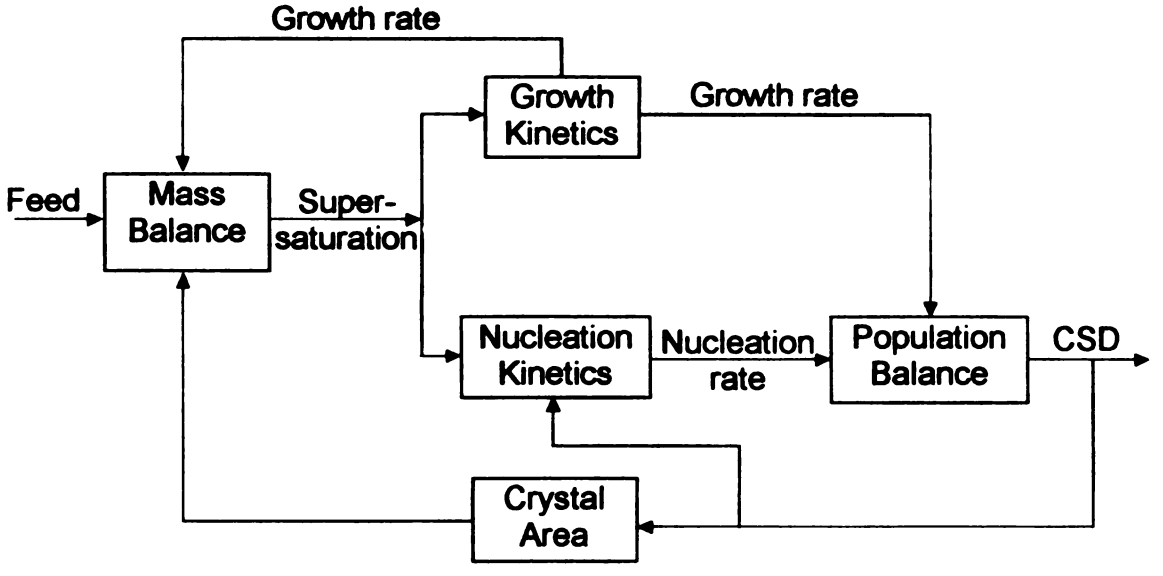

Figure 1.1. Feedback diagram to demonstrate the complex interaction between crystal size distribution and factors that form the crystal size distribution [44].

variety of different products and the crystallizer is easy to clean between batches. Cleaning is necessary to prevent contamination from batch to batch. Other advantages of batch crystallization include low level of maintenance, and particular suitability for difficult processes, like processing of toxic materials or exclusion of contaminants. Batch crystallizers can also produce a narrower crystal size distribution (Wey [59]). However, the analysis of a batch process is considerably more complex than that of a continuous system due to the dynamic nature of the batch process. Also batch-to-batch fluctuations pose a problem in batch processing, which can cause considerable variation in the crystallization process resulting in final product divergence. Such variation is unacceptable in the pharmaceutical industry. Reworking a batch that does not meet the specifications is time consuming and expensive, and it opens the opportunity for additional contamination.

1.3.2 Controlled operation of batch crystallizers

Batch crystallizers are generally operated under one of the following three modes: cooling crystallization, evaporative crystallization, or antisolvent crystallization (Mullin [34]). The aim of the controlled operation of a crystallizer is to obtain a desired crystal size distribution. In cooling and evaporative crystallization this is achieved by controlling the level of supersaturation in the crystallizer.

Operating a batch cooling crystallizer under a natural cooling profile without any temperature control is known to produce a supersaturation peak in the crystallizer. This peak causes a burst of nucleation that leads to excessive formation of very small particles (fines) and small average crystal sizes. These small crystals, in turn, lead to fouling problems, reduced product yields, and problems in downstream product handling (Mullin [34]). To avoid this problem, the crystallizer is operated according to an established cooling curve, i.e. the cooling rate is small initially and is gradually increased towards the end of the batch. This approach keeps the level of supersaturation constant in the crystallizer and prevents excessive nucleation. The

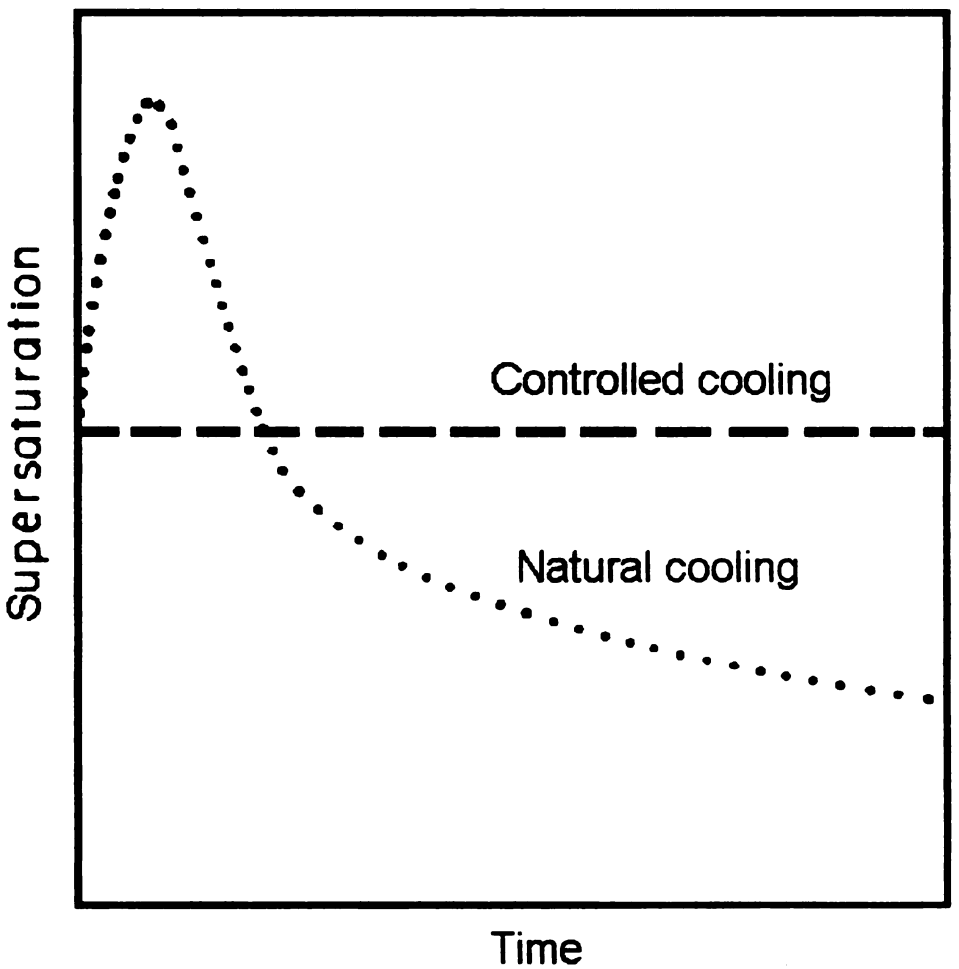

Figure 1.2. Supersaturation profiles for natural and controlled cooling (Mullin [34]).

supersaturation profiles obtained from uncontrolled (natural) and controlled cooling are shown in Figure 1.2.

A similar strategy is used for evaporative batch crystallization processes. In this case, the controlled operations involve operating the crystallizer initially at a lower evaporation rate and then gradually increasing it. The problems occurring due to natural evaporation are the same as for natural cooling described earlier.

1.4 Batch antisolvent crystallization

1.4.1 Introduction

A batch crystallization operation commonly used in the pharmaceutical and biochemical industry is antisolvent crystallization. Numerous amino acids, including proline, l-asparagine, and l-alanine, and pharmaceuticals, including antibiotics, are crystallized using antisolvent crystallization (Kirwan and Orella [25]). In antisolvent crystallization a solute is crystallized from solution by the addition of another substance (a soluble solid, liquid or gas). The added substance effectively reduces the solubility of the solute in the original solvent, and thus increases the supersaturation. This type of crystallization is known by a variety of terms. When the added substance is another liquid and the solute is organic, like in pharmaceutical crystallizations, the term antisolvent crystallization is used. Also terms like salting-out, diluent crystallization, and watering-out are used. Salting-out and diluent crystallization usually refer to inorganic solutes, and watering-out can be used when the antisolvent is water.

The advantages of antisolvent crystallization are many. The major advantage is the possibility to perform the crystallization at low temperature which is essential when heat sensitive solutes, like amino acids, are crystallized. This method also produces narrow crystal size distributions.

Further advantages that can be obtained by the right choice of antisolvent are high purity crystals (Karpinski [23]) and high yield. The disadvantage of the technique is that, usually, a separation unit is required to recover the added antisolvent.

1.4.2. Choice of solvents

In crystallization the choice of solvent is important. The solvent can have a major effect on the growth rate and the crystal habit, and therefore also on the crystal size distribution (Myerson et al. [37], Davey [10]). Also, the choice of solvent can affect the solubility of the solute significantly. Figure 1.3 demonstrates the effect of various solvents on the solubility of adipic acid in various solvents (Myerson [36]).

Choosing the antisolvent should also be done carefully. The antisolvent should be miscible with the original solvent over the ranges of concentrations encountered and the solute should be relatively insoluble in it. Also, the final solvent-antisolvent mixture must be readily separable. Figure 1.4 shows the effect of addition of iso-propanol on the solubilities of some aqueous solutions of amino acids (Kirwan and Orella [25]). These data demonstrate that the right choice of solvent can decrease the solubility of the solute by orders of magnitude, and indicates the possibility of high solute yields.

1.4.3 Amino acid salt recrystallization

The system that was chosen for this research is the purification of l-lysine monohydrochloride from aqueous solution using ethanol as an antisolvent. X-ray crystallography was used to confirm that ethanol does not change the crystal structure of l-lysine monohydrochloride. L-lysine (2,6-diaminohexanoic acid) is an essential amino acid that has been shown to affect the growth of rats (Budavari [3]). It is often the limiting amino acid in animal nutrition, and thus it is added to animal feed (Kirk-Othmer [24]). It is also an essential part of pre- and post-operational nutrition

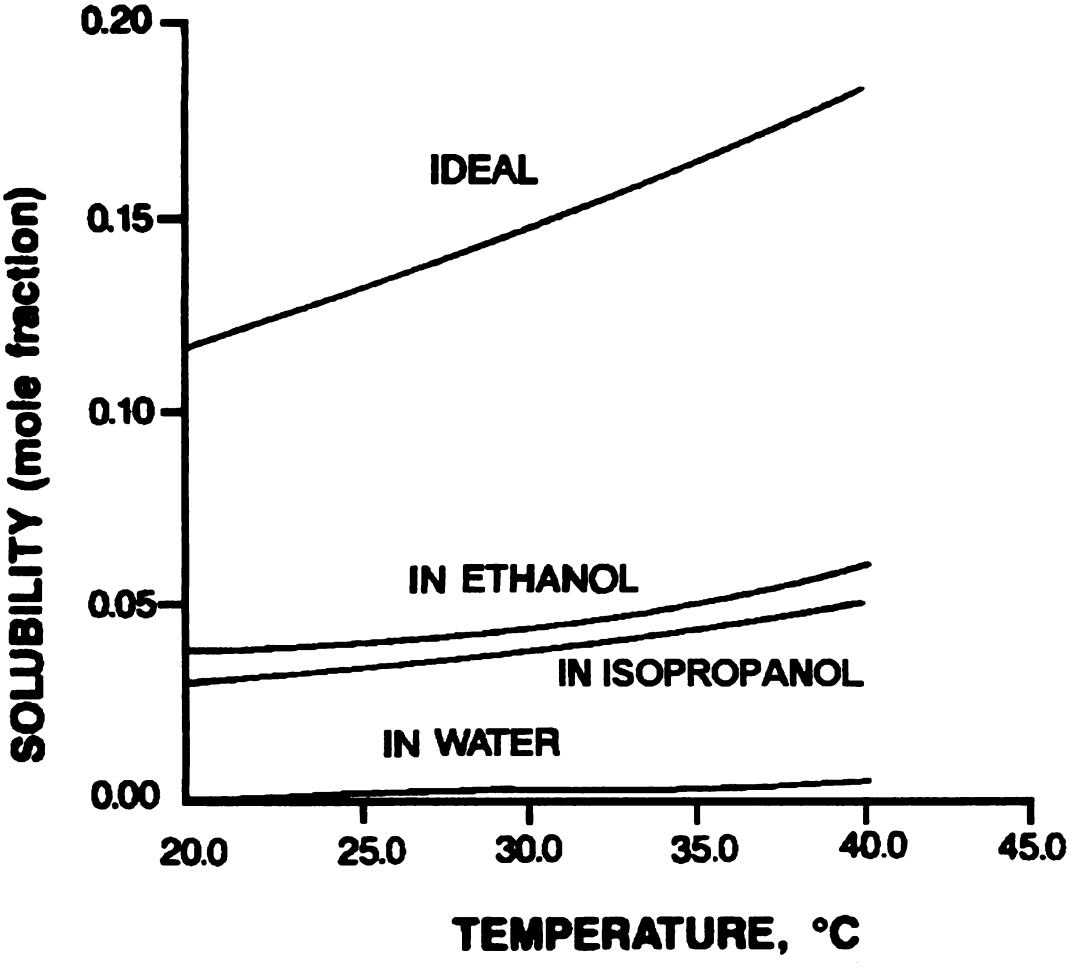

Figure 1.3. Solubility of adipic acid in different solvents (Myerson [36]).

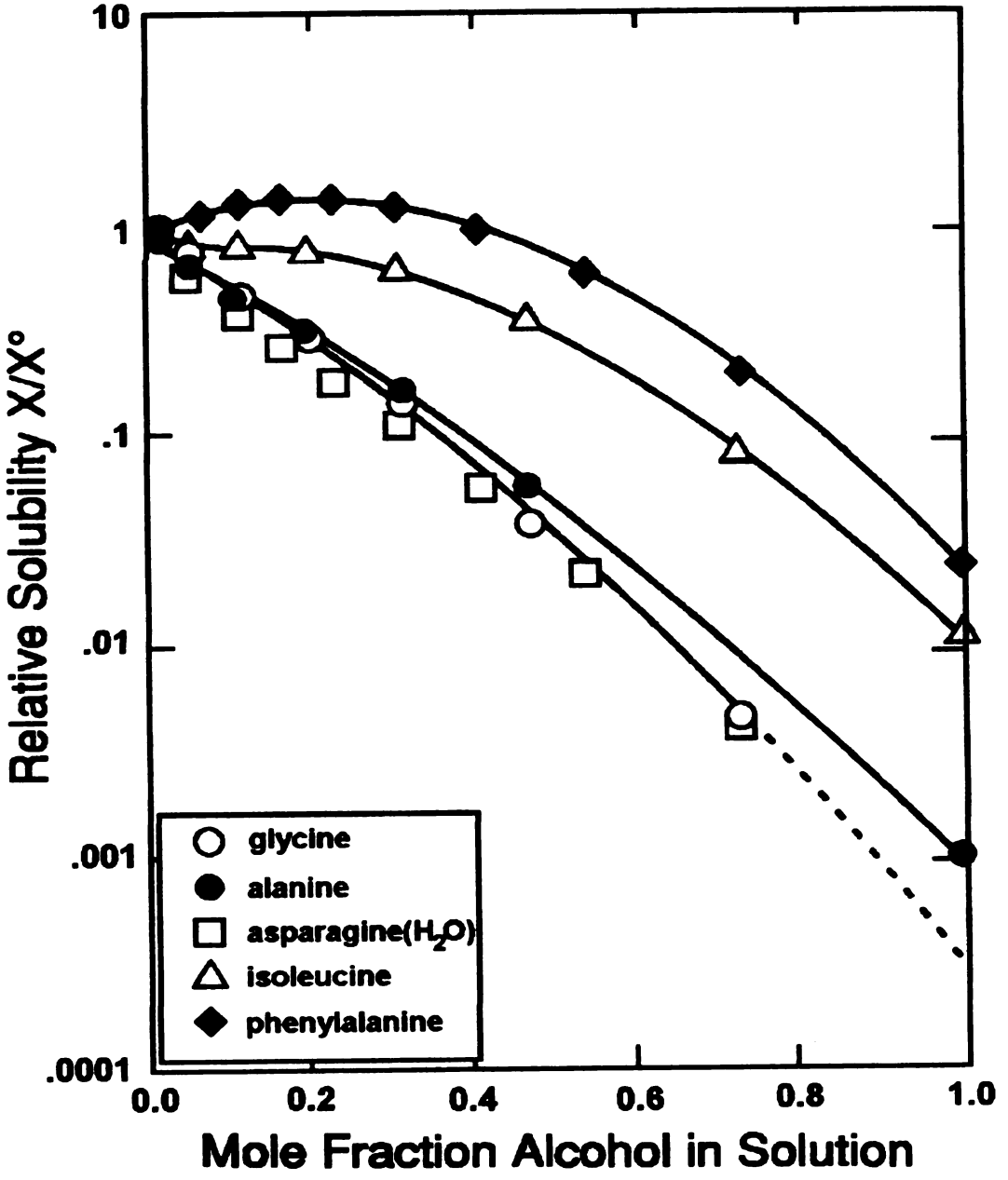

Figure 1.4. The solubility of various amino acids in aqueous 1-propanol solutions [42].

for humans. This system was chosen as a model of a pharmaceutical crystallization. L-lysine monohydrochloride is easy to crystallize, and it is freely soluble in water and very slightly soluble in ethanol.

1.5 Polarity changes in binary systems

In the case of batch antisolvent crystallization, there is very little published information on operating strategies; even though the technique is commonly used for the production of pharmaceuticals and amino acids. Most of the related research is done for continuous crystallization (for example, Bátor [2], Mina-Mankarios and Pinder [31]). There are a few batch studies, but they are done using inorganic solutes (Budz et al. [4], Jones and Teodossiev [22], Jones et al. [21], Karpinski and Nývlt [23], Mullin et al. [35], and Tavare and Chivate [54]). There are two more closely related studies. Gabas and Laguérie [15] have studied the antisolvent crystallization of D-xylose. They add only 1 w-% of antisolvent, and consequently assume that the change in solubility is linear. This makes it difficult to generalize their results. Nývlt's study [40], on the other hand, is theoretical. Both of these studies assume that the solvation of the solute is a simple competition between the two solvents. However, when the two solvents are of significantly different polarity, the solvation is affected by nonlinear polarity changes due to either dielectric enrichment effect or hydrogen bonding. There is a vast amount of literature available on this topic (Ghoneim and Suppan [16], Midwinter and Suppan [30], Nitsche and Suppan [39], Reichardt [45], Suppan [50, 51, 52]). These solvent effects cause the local polarity around the solute molecule to differ significantly from the bulk polarity of the mixture. This makes the system more complex than that assumed by Gabas and Laguérie [15] and Nývlt [40], and the optimal operating conditions will not be achieved using these approaches. Thus, instead of assuming ideal behavior of solvents, the nonlinear polarity changes can be exploited in developing the operating strategy for antisolvent crystallization.

Chapter 2

SPECTROSCOPICALLY DETERMINED DIELECTRIC CONSTANTS FOR VARIOUS ESTERS

2.1 Introduction

The polarity of a solvent can be defined by the Onsager function or the Debye function. They are both functions of the static dielectric constant of a solvent (Ghoneim and Suppan [16], Suppan [52]). Polarity has also been shown to be related to the solvatochromic shifts of the absorption and fluorescence spectra (Dutta et al. [14], Suppan [51]). Using a polarity sensitive solvatochromic probe molecule, such as Nile Red [14], the Onsager function and the Debye function can be correlated with the peak shifts in the emission maxima of Nile Red. These correlations can then be used to estimate dielectric constants for various less known solvents, like dibasic esters.

The emission maxima of the probe molecule Nile Red are measured in different solvents of known dielectric constants, and relationships between the emission maxima and the Onsager and Debye functions are established. Both the Onsager function and the Debye function will give a linear relationship when correlated with either the maximum absorption wavelength of Nile Red or the maximum emission wavelength of Nile Red. These plots can be used to estimate dielectric constants for less known solvents.

This chapter follows closely the article "Spectroscopically determined dielectric constants for various esters" by Uusi-Penttilä et al. [57].

2.2 Experimental procedure

2.2.1 Chemicals

The following solvents were used to determine the linear relationship between the emission maxima of Nile Red and the two polarity functions: methanol (absolute) from Mallinckrodt; ethanol (anhydrous) from Quantum Chemical Corporation; n-propanol (anhydrous), n-octanol (99+%), and ethyl acetate (absolute) from J.T. Baker; n-butanol (99+%), n-pentanol (99+%), n-hexanol (98%), ethyl acetoacetate (99%), ethyl formate (97%), propyl formate (97%), butyl acetate (99%), methyl propionate (99%), and methyl butyrate (99%) from Aldrich. Nile Red was also from Aldrich.

The dielectric constants were determined for the following less known solvents: dimethyl succinate (98+%), dimethyl glutarate (98+%) and dimethyl adipate (98+%) that were graciously supplied by Du Pont; diethyl succinate (99%), diethyl maleate (97%), diethyl fumarate (98%), diethyl l-tartrate (99+%), dibutyl maleate (97%), dibutyl l-tartrate (99%), ethyl l-lactate (98%), and triethyl citrate (99%) from Aldrich; dibutyl itaconate from Lancaster; dibutyl fumarate (90%) from Kodak; and dimethyl maleate (Baker grade) from J.T. Baker. All chemicals were used without further purification.

2.2.2 Instrumentation

The equipment used for absorption measurements was a Perkin-Elmer Lambda 3A UV-Vis Spectrophotometer, and the fluorescence experiments were performed on a SPEX FLUOROLOG 1681 0.22 m Spectrometer. Quartz cuvettes were used for both absorption and emission experiments. The accuracy for both the absorption and emission spectra were ±1 nm.

2.2.3 Sample preparation

The esters possess a strong characteristic absorption below 350 nm that saturate the absorption instrument. Therefore, Nile Red that absorbs and emits at considerably higher wavelengths was used as a solvatochromic probe. According to Deye and Berger [11] and Dutta et al. [14], Nile Red is very sensitive to the polarity of the medium in which it is located. Nile Red has also been found to be very soluble and strongly fluorescent in organic solvents (Greenspan and Fowler [17]).

Nile Red is only needed in trace amounts for the measurements. Thus, a method described in Street and Acree [49] was used to ensure the accuracy of the Nile Red concentration. A 10^{-3} M stock solution of Nile Red was prepared by dissolving 0.00636 g of Nile Red in 20 ml of spectroscopic grade methanol. The stock solution was pipetted into vials. 50 µl of stock solution was used for absorption sample vials and 10 µl for emission sample vials. These will yield final Nile Red concentrations of 10^{-5} M for absorption samples and $2*10^{-6}$ M for the emission samples. The solvent was allowed to air dry, leaving the appropriate amount of Nile Red in the vial, and the Nile Red was redissolved in 5 ml of a chosen solvent.

2.3 Results

2.3.1 Absorption versus emission

As expected from the abundant literature on this subject (Suppan [53, 54], Ghoneim and Suppan [16], Onsager [41]), no general polarity scale can be established on the basis of solvatochromic shifts of a probe. However, within categories of solvents, such as alcohols or esters, the absorption and emission peak shifts follow a trend. These trends can be correlated with the

polarity of the solvent that is reflected by the static dielectric constant of that solvent, *D*, through either the Onsager function or the Debye function (Suppan [53, 54], Onsager [41]).

Onsager function	$f(D) = 2\,(D\text{-}1) / (2D\text{+}1)$	2.1
Debye function	$\varphi(D) = (D\text{-}1) / (D\text{+}2)$	2.2

Fluorescence spectroscopy was chosen here rather than absorption spectroscopy because of its enhanced sensitivity, i.e. larger peak shifts (Ghoneim and Suppan [16]). This is demonstrated in Figure 2.1 where the absorption peaks for the chosen esters and alcohols fall within the range of 519 nm and 557 nm (38 nm) whereas the emission peaks cover the range from 583 nm to 640 nm (57 nm). The linear correlation between absorption and emission peaks is given in Equation 2.3. As can be seen from the equation, emission gives about 1.5 times larger peak shifts than absorption.

$$\lambda_{emission} = -225 + 1.57 * \lambda_{absorption} \qquad (r^2 = 0.88) \qquad 2.3$$

2.3.2 Onsager and Debye functions

The relationships between the two functions and the Nile Red emission maxima were established. Since some of the esters studied here contain hydroxyl groups both esters and alcohols were included in the correlations. Using only the esters for the correlations would considerably underestimate the values of the dielectric constants for esters containing hydroxyl groups, whereas using only the alcohol data the lower dielectric constants could not be estimated using this method. Combining the two groups gave the most consistent results for both the high and the low end of the dielectric constants.

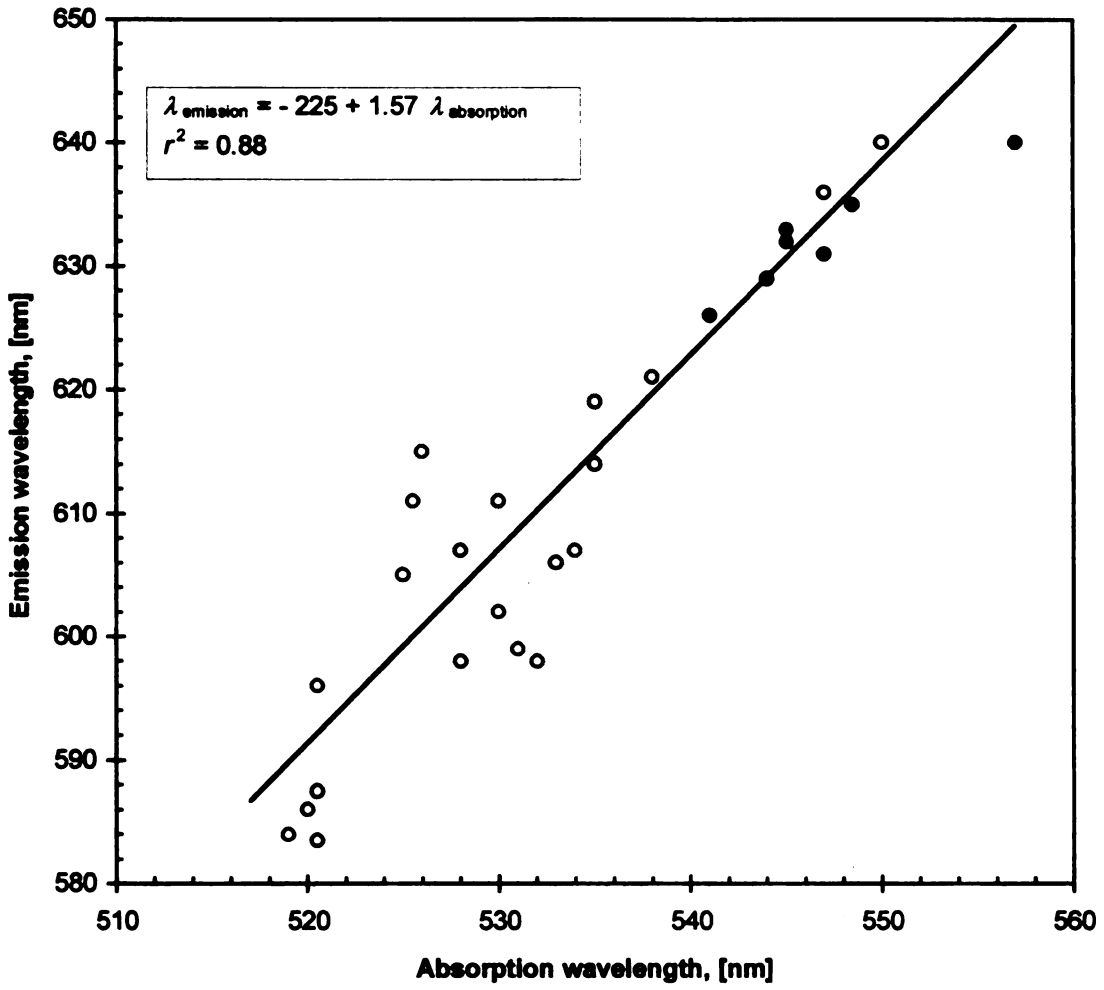

Figure 2.1. Nile Red emission maxima as a function of Nile Red absorption maxima in various esters (o) and alcohols (•). The emission spectra were excited at absorption maxima.

The best linear correlations were obtained when the excitation was performed at the wavelength of the maximum Nile Red absorption peak for each sample. Nile Red emission spectra were recorded for pure solvents of known dielectric constants. The Onsager and Debye functions were calculated from Equations 2.1 and 2.2 and plotted as a function of the Nile Red emission maxima. The plots are shown in Figure 2.2 and the numerical data are presented in Table 2.1. The linear equations were generated in EXCEL by a least squares treatment of the data.

$$f(D) = -1.45 + 0.0037 * \lambda_{emission} \qquad (r^2 = 0.95) \qquad 2.4$$

$$\varphi(D) = -2.66 + 0.0055 * \lambda_{emission} \qquad (r^2 = 0.94) \qquad 2.5$$

The linear relationships in Figure 2.2 were then used to predict the dielectric constants for chemically similar substances of unknown dielectric constants. The emission spectrum of Nile Red in a solvent of unknown dielectric constant was recorded by exciting at the absorption maximum. Figure 2.2 was used to determine the values for the Onsager and the Debye functions and the dielectric constant of the solvent was calculated from Equations 2.1 and 2.2. The resulting dielectric constants for selected solvents are presented in Figure 2.3 and in Table 2.2.

$$D = (f(D) + 2) / [2 (1 - f(D))] \qquad 2.1$$

$$D = [1 + 2 \varphi(D)] / [1 - \varphi(D)] \qquad 2.2$$

2.4 Discussion

Despite a comprehensive literature search, direct measurement of dielectric constants for ethyl lactate, triethyl citrate and many dibasic esters, that are considered as environmentally benign

substitutes for various chlorinated solvents, were not found. The spectroscopic approach was found to provide an easy, experimental method to estimate static dielectric constants of less common solvents.

It can be seen from Figure 2.3 that both the Onsager function and the Debye function give very similar results. Thus, for the systems studied here neither model is superior. The scatter in Figure 2.3 also shows that because of the exponential nature of the two models, the smaller values of the dielectric constant are more reliable than the larger values. For dielectric constants up to 15 this method tends to underestimate the value of the dielectric constant up to 15 %. For higher values of dielectric constants this method tends to overestimate the values, about 25 % at dielectric constant of 25, and the error increases towards the higher values of dielectric constants.

The accuracy of the estimated dielectric constants was compared with other related results from literature. An earlier publication by Smyth and Walls [47] gives electric moments for dilute solutions of ethyl formate, ethyl acetate, diethyl maleate, diethyl fumarate, and diethyl succinate in benzene. Extrapolation of their results to obtain the dielectric constants for pure solvents agrees well with the results presented here. Further comparison was done with the results of Stolarová et al. [48]. They have published values for various solvent polarity parameters including results on diethyl maleate and ethyl lactate. The function they have used is similar to the two functions used in this thesis. Thus, the dielectric constants they have used are easily reproduced. Their value for diethyl maleate is in good agreement with the results presented here. The value for ethyl lactate differs some from the estimate here. This was expected based on the bigger errors in the estimation of the larger values of dielectric constants. These values from Smyth and Walls [47] and Stolarová et al. [48] are also presented in Tables 2.1 and 2.2.

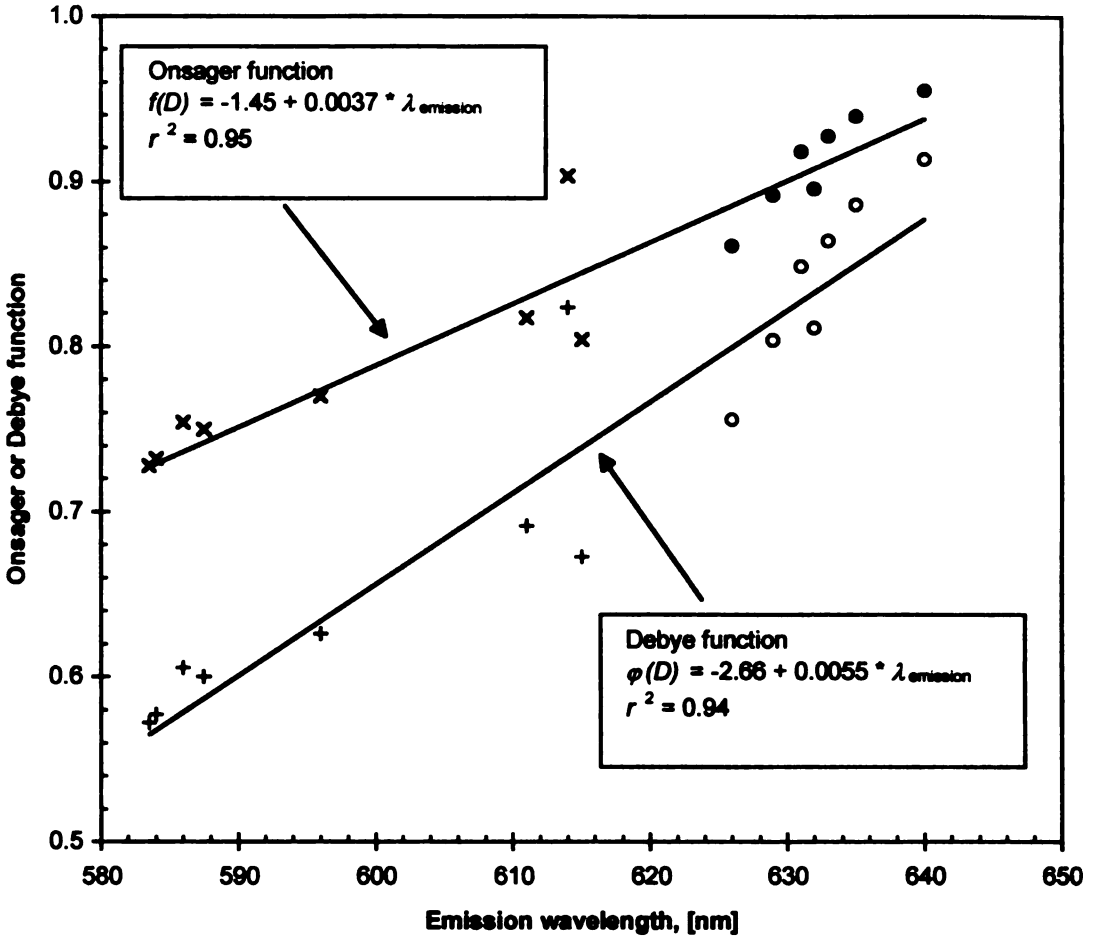

Figure 2.2. *f(D)* and *φ(D)* for solvents of known dielectric constant as a function of the emission wavelength of Nile Red (alcohols (•) and esters (x) for *f(D)*, and alcohols (o) and esters (+) for *φ(D)*).

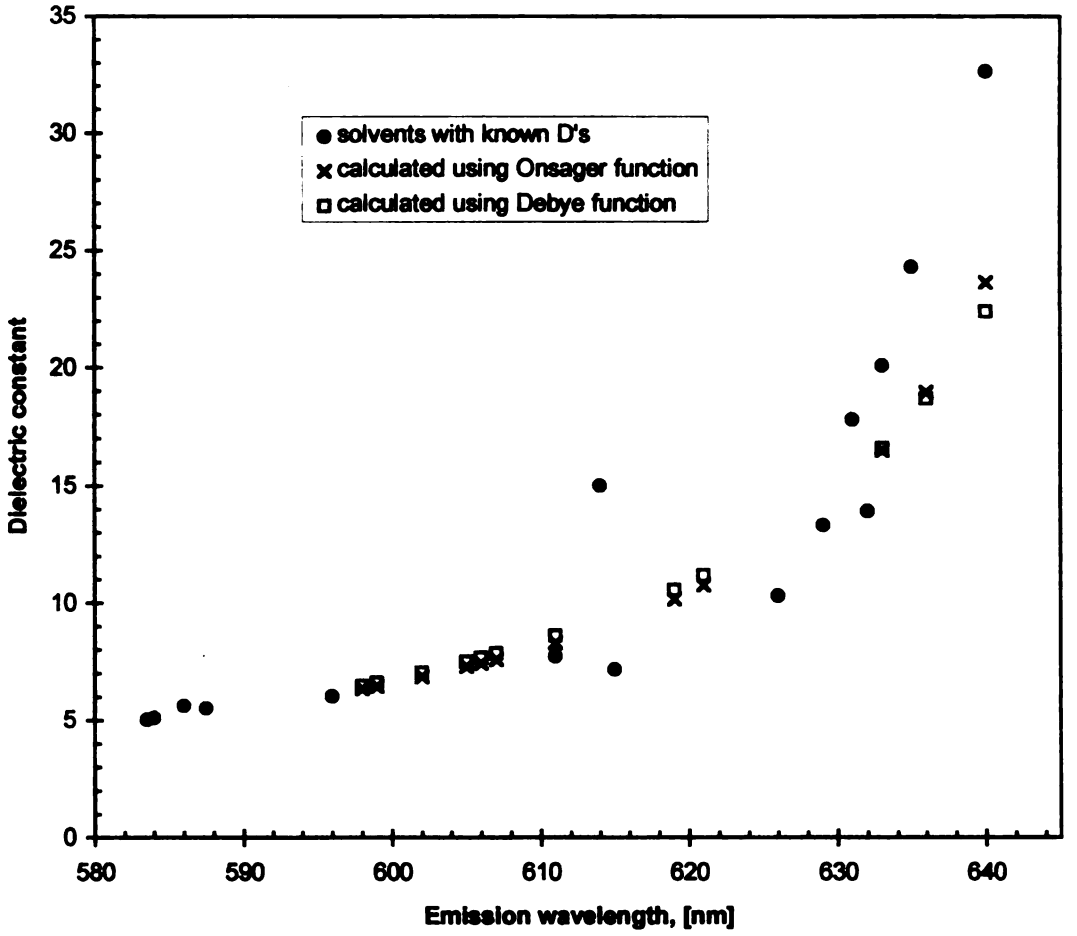

Figure 2.3. Dielectric constant as a function of Nile Red emission maximum.

Table 2.1. The emission maxima for Nile Red in the various solvents of known dielectric constants. The values for the Onsager function, *f(D)*, are calculated from Equation 2.1; for the Debye function, $\varphi(D)$, from Equation 2.2, and the dielectric constants have been obtained from CRC Handbook of Chemistry and Physics [26]. The comparisons in the last column are: [a] from Smyth and Walls [47], and [b] from Stolarová et al. [48].

SOLVENT	EMISSION	*f(D)*	$\varphi(D)$	*D*	$D^{a,b}$
methanol	640 nm	0.955	0.913	32.63	32.1[b]
ethanol	635 nm	0.940	0.886	24.30	24.5[b]
n-propanol	633 nm	0.927	0.864	20.10	20.3[b]
n-butanol	631 nm	0.918	0.848	17.80	17.4[b]
n-pentanol	632 nm	0.896	0.811	13.90	13.9[b]
n-hexanol	629 nm	0.891	0.804	13.30	13.4[b]
n-octanol	626 nm	0.861	0.756	10.30	10.4[b]
ethyl formate	615 nm	0.804	0.672	7.16	7.2[a], 7.2[b]
propyl formate	611 nm	0.818	0.691	7.72	7.7[b]
ethyl acetate	596 nm	0.770	0.626	6.02	6.3[a], 6.0[b]
ethyl acetoacetate	614 nm	0.903	0.824	15.00	
butyl acetate	584 nm	0.728	0.572	5.01	5.0[b]
methyl propionate	588 nm	0.750	0.600	5.50	5.5[b]
methyl butyrate	586 nm	0.754	0.605	5.60	
ethyl butyrate	584 nm	0.732	0.577	5.10	5.1[b]

Table 2.2. The emission maxima for Nile Red in various esters of unknown dielectric constants. The values for the Onsager and Debye functions using Figure 2.2, and the respective dielectric constants calculated from Equations 2.1 and 2.2. The comparisons in the last column are: [a] from Smyth and Walls [47], and [b] from Stolarová et al. [48].

ESTER	EMISSION	*f(D)*	*φ(D)*	*D(f(D))*	*D(φ(D))*	$D^{a,b}$
ethyl lactate	636 nm	0.92	0.85	19	19	13.1[b]
dimethyl succinate	606 nm	0.81	0.69	7.4	7.5	7.8[a]
dimethyl maleate	621 nm	0.87	0.77	11	11	
dimethyl glutarate	605 nm	0.81	0.68	7.3	7.5	
dimethyl adipate	602 nm	0.80	0.67	6.9	7.0	
diethyl succinate	599 nm	0.78	0.65	6.5	6.6	
diethyl maleate	607 nm	0.81	0.69	7.6	7.8	10[a], 8.5[b]
diethyl fumarate	598 nm	0.78	0.64	6.4	6.5	9.5[a]
diethyl l-tartrate	640 nm	0.94	0.88	24	22	
dibutyl fumarate	607 nm	0.81	0.69	7.6	7.8	
dibutyl l-tartrate	633 nm	0.91	0.84	16	17	
dibutyl itaconate	598 nm	0.78	0.64	6.4	6.5	
dibutyl maleate	611 nm	0.83	0.72	8.3	8.6	
triethyl citrate	619 nm	0.86	0.76	10	11	

2.5 Conclusions

Nile Red emission was recorded in various solvents of known polarity, and a linear relationship was found when the Onsager function and the Debye function were plotted as a function of the emission maxima of Nile Red. This relationship was used to estimate dielectric constants for some dibasic esters, triethyl citrate, and ethyl lactate. The results agree well with related publications. Thus, the approach provides a convenient experimental method to estimate static dielectric constants of some less common organic solvents.

Chapter 3

POLARITY IN BINARY SYSTEMS

3.1 Introduction

Chapter 2 presented an experimental method to estimate dielectric constants for less known solvents. The same approach will be used here to determine polarity changes in binary systems. The binary systems will be studied using fluorescence spectroscopy. A polarity sensitive solvatochromic probe, Nile Red, will be used to indicate changes in the polarity of the system.

This chapter follows loosely a manuscript "Dielectric enrichment in binary systems containing environmentally benign esters" by Uusi-Penttilä et al. [58].

3.2 Experimental

3.2.1 Chemicals

Ethanol (anhydrous) was from Quantum Chemical Corporation. Diethyl succinate (99%), diethyl maleate (97%), diethyl fumarate (98%), ethyl l-lactate (98%), and Nile Red were purchased from Aldrich. HPLC grade water from Fisher Scientific Company was used in the experiments. All chemicals were used without further purification.

3.2.2 Instrumentation

The equipment used for absorption measurements was a Perkin-Elmer Lambda 3A UV-Vis Spectrophotometer, and the fluorescence experiments were performed on a SPEX FLUOROLOG 1681 0.22 m Spectrometer. Quartz cuvettes were used in all the experiments. The accuracy of both the absorption and emission spectra were ±1 nm.

3.2.3 Sample preparation

A trace amount of Nile Red was needed for the experiments, i.e. 10^{-5} M of Nile Red for absorption experiments and $2*10^{-6}$ M for emission experiments. For greater accuracy, Nile red was diluted according to a procedure described in Chapter 2.2.3. Binary mixtures were prepared on volume basis dissolving the Nile Red first into the solvent that it was more soluble in.

3.3 Results

In Uusi-Penttilä et al. [57] the absorption and emission maxima of Nile Red in pure solvents have been determined. In the same paper the dielectric constants have been calculated for pure solvents using both the Onsager model and Debye model [39], [53]. The best linear correlation between the emission maxima and the two models were obtained when the samples were excited at their respective absorption maxima.

The same approach was used for binary systems. The emission spectra of Nile Red, excited at absorption maxima, were taken for five binary systems: diethyl succinate-ethanol, diethyl fumarate-ethanol, diethyl maleate-ethanol, ethyl lactate-water, and ethanol-water. The results are presented in Figures 3.1-3.5 and in Tables 3.1-3.5. The dots represent the experimental

emission maxima of Nile Red and the straight line indicates the linear addition of polarities for ideal systems.

The experimental values presented in Figures 3.1-3.5 differ considerably from the ideal linear relation of polarities. According to Midwinter and Suppan [30], this can be caused by either of two effects: the dielectric enrichment or hydrogen bonding. They have determined that the dielectric enrichment causes a red shift in the absorption and emission maxima, i.e. a shift to higher wavelength, and hydrogen bonding causes a blue shift, i.e. a shift to lower wavelength. They have also concluded that in the case of hydrogen bonding there may be a threshold value below which the addition of the second solvent does not effect the hydrogen bonding enough to change the spectrum. These effects have to be accounted for when working with binary systems.

The first three systems in Figures 3.1-3.3 demonstrate the dielectric enrichment effect. They all show a slight shift of the Nile Red emission maxima toward higher wavelengths. However, the ethyl lactate-water system in Figure 3.4 and the ethanol-water system in Figure 3.5 deviate from ideality toward lower wavelengths. The dielectric constant of ethanol is 24 [26], and in Chapter 2 the dielectric constant for ethyl lactate was estimated to be 19. Figures 3.4 and 3.5 clearly show that the ethyl lactate-water system with a bigger difference in the dielectric constants is significantly less ideal than the ethanol-water system. However, in both cases, the less polar solvent has a considerable effect on the hydrogen bonding of water, and even small amounts of ethyl lactate or ethanol will cause large changes in the local polarity of the system.

3.4 Discussion

The polarity behavior of binary mixtures including two solvents of considerably different dielectric constants is nonideal. The polarities of the pure solvents in a binary mixture are not additive since the polarity change is not linear. This can be accounted for either by dielectric enrichment

Table 3.1. Nile Red emission maxima for diethyl succinate-ethanol binary mixture as a function of the mole fraction of diethyl succinate at 25 °C. The accuracy is ±1 nm.

Mole fraction of diethyl succinate	Nile Red emission maximum, [nm]	Mole fraction of diethyl succinate	Nile Red emission maximum, [nm]
0.000	635	0.355	629
0.039	635	0.594	624
0.084	634	0.767	618
0.196	632	1.000	599

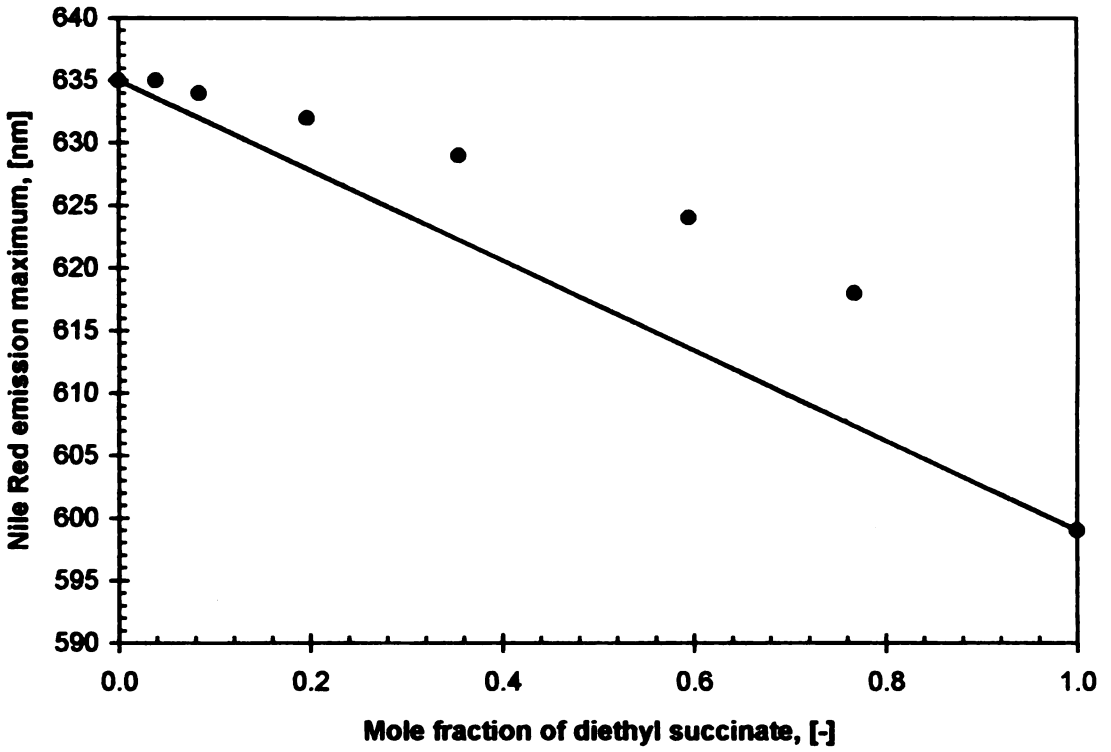

Figure 3.1. The emission maxima of Nile Red in differing mole fractions of diethyl succinate in ethanol. The straight line represents the ideal behavior of the system.

Table 3.2. Nile Red emission maxima for diethyl fumarate-ethanol binary mixture as a function of the mole fraction of diethyl fumarate at 25 °C. The accuracy is ±1 nm.

Mole fraction of diethyl fumarate	Nile Red emission maximum, [nm]	Mole fraction of diethyl fumarate	Nile Red emission maximum, [nm]
0.000	635	0.358	630
0.040	634	0.598	625
0.085	633	0.770	618
0.199	632	1.000	598

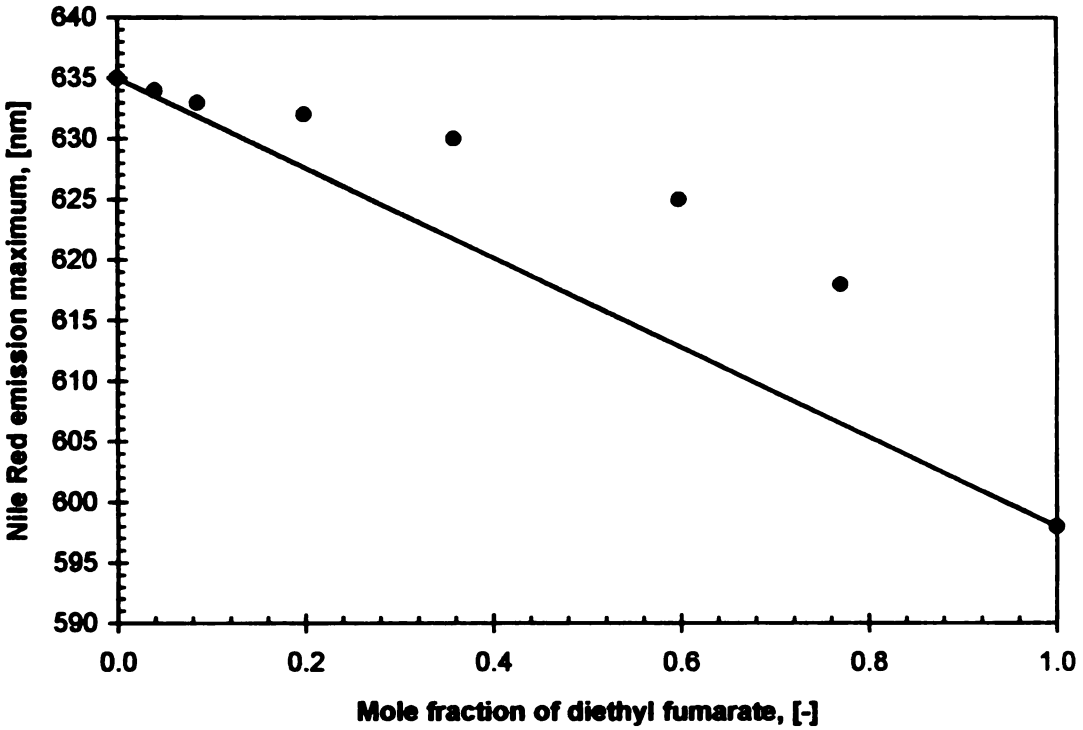

Figure 3.2. The emission maxima of Nile Red in differing mole fractions of diethyl fumarate in ethanol. The straight line represents the ideal behavior of the system.

Table 3.3. Nile Red emission maxima for diethyl maleate-ethanol binary mixture as a function of the mole fraction of diethyl maleate at 25 °C. The accuracy is ±1 nm.

Mole fraction of diethyl maleate	Nile Red emission maximum, [nm]	Mole fraction of diethyl maleate	Nile Red emission maximum, [nm]
0.000	635	0.361	633
0.040	636	0.601	629
0.086	636	0.772	624
0.201	635	1.000	607

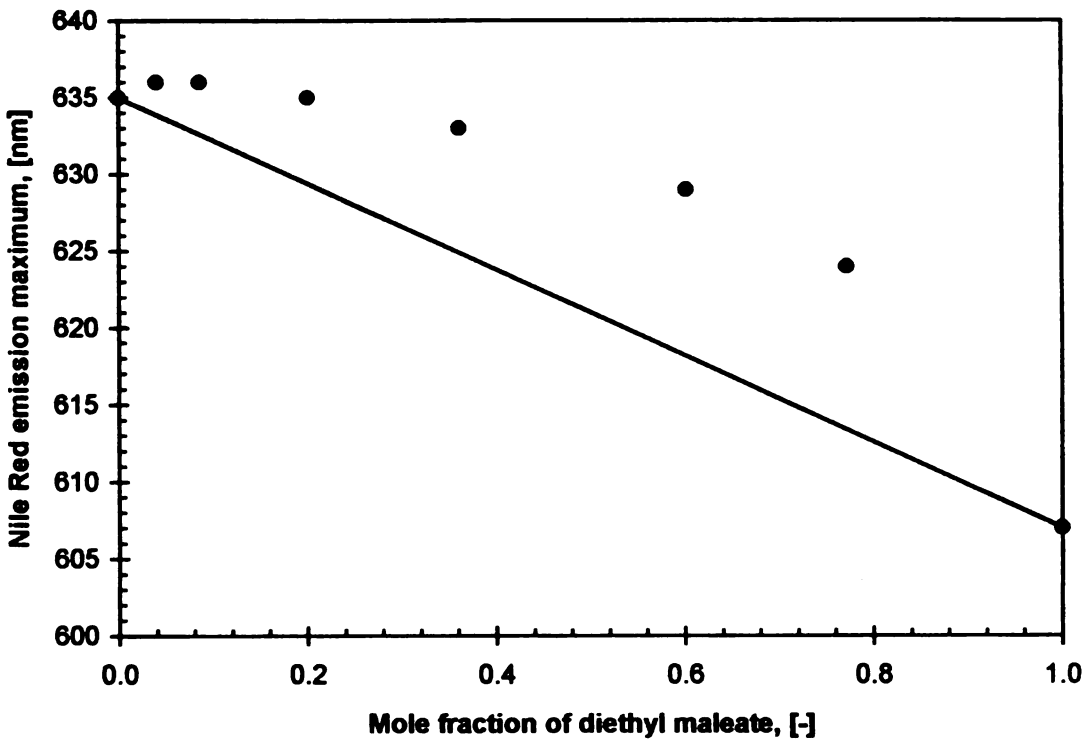

Figure 3.3. The emission maxima of Nile Red in differing mole fractions of diethyl maleate in ethanol. The straight line represents the ideal behavior of the system.

Table 3.4. Nile Red emission maxima ethyl lactate-water binary mixture as a function of the mole fraction of ethyl lactate at 25 °C. The accuracy is ±1 nm.

Mole fraction of ethyl lactate	Nile Red emission maximum, [nm]	Mole fraction of ethyl lactate	Nile Red emission maximum, [nm]
0.000	670	0.193	649
0.017	661	0.389	645
0.038	659	0.589	642
0.096	653	1.000	636

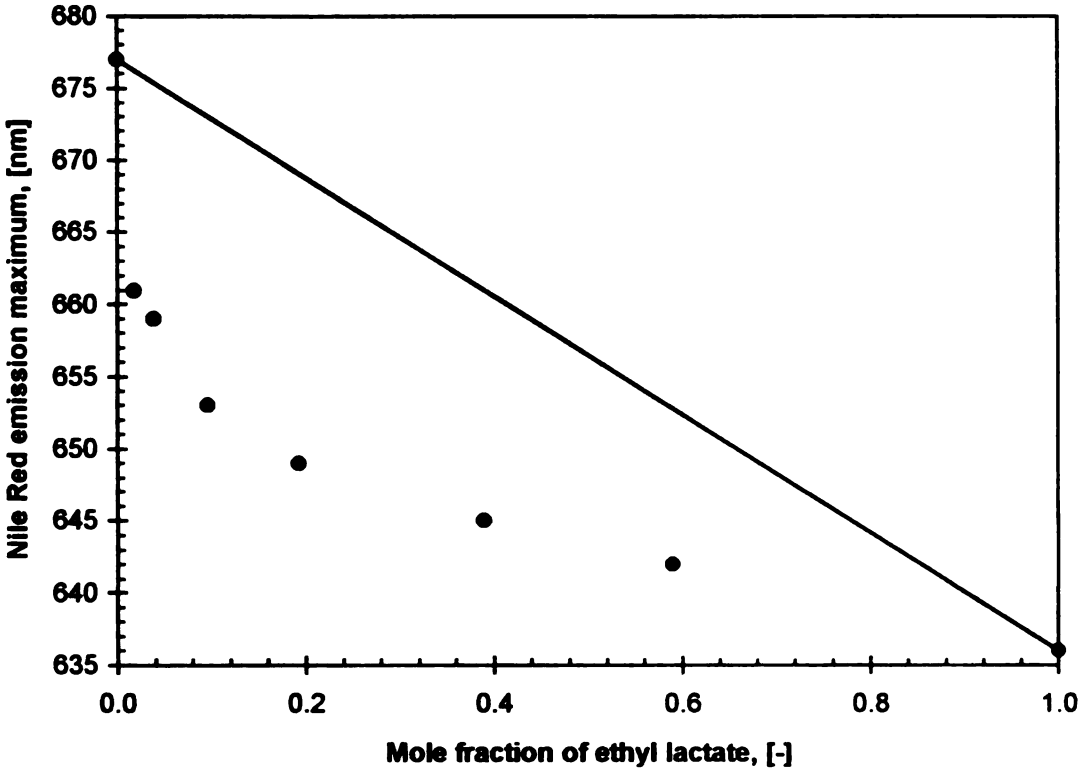

Figure 3.4. The emission maxima of Nile Red in differing mole fractions of ethyl lactate in water. The straight line represents the ideal behavior of the system.

Table 3.5. Nile Red emission maxima for ethanol-water binary mixture as a function of the mole fraction of ethanol at 25 °C. The accuracy is ±1 nm.

Mole fraction of ethanol	Nile Red emission maximum, [nm]	Mole fraction of ethanol	Nile Red emission maximum, [nm]
0.000	677	0.227	650
0.032	666	0.407	649
0.068	662	0.540	645
0.112	660	0.726	641
0.164	655	1.000	636
0.439	652		

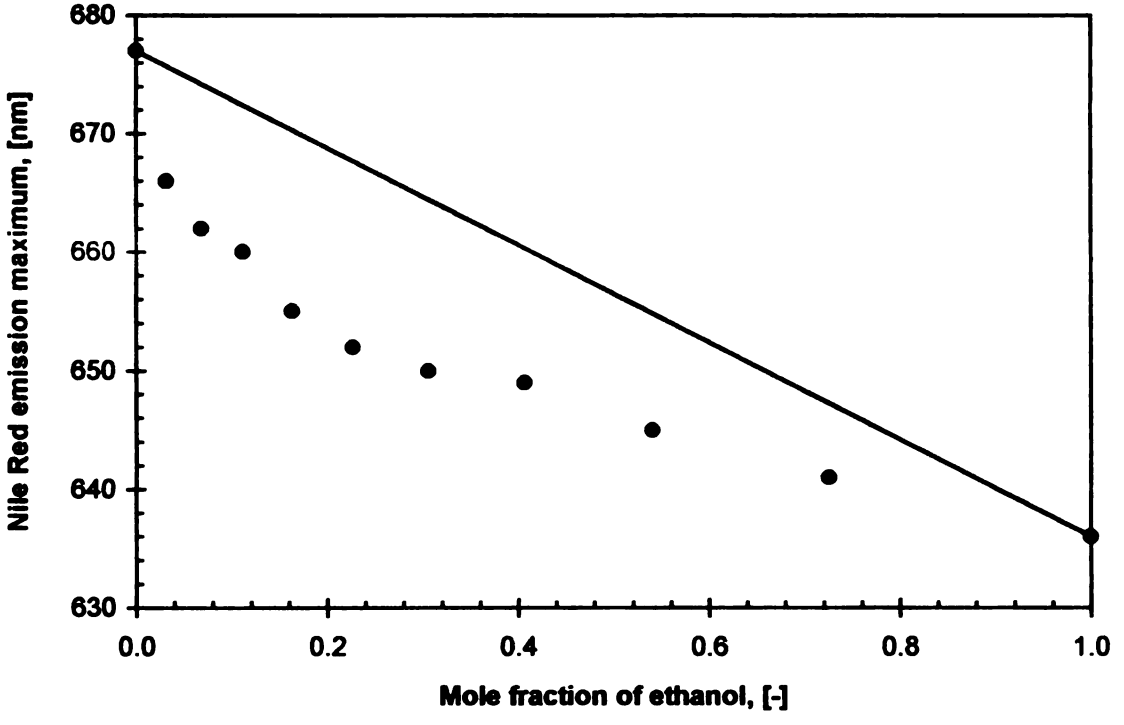

Figure 3.5. The emission maxima of Nile Red in differing mole fractions of ethanol in water. The straight line represents the ideal behavior of the system.

effect or by hydrogen bonding. The dielectric enrichment effect can be seen from Figures 3.1-3.3 where a small amount of the less polar solvent causes a much smaller change in the system polarity than would be expected. Similarly, adding a small amount of the more polar solvent into the less polar solvent causes a dramatic change in the system polarity. However, as can be seen from Figures 3.4 and 3.5, the hydrogen bonding causes an opposite effect. The addition of the less polar solvent decreases the polarity of the system considerably; whereas, adding the more polar solvent into the less polar solvent hardly changes the polarity.

3.5 Conclusions

Five binary systems were studied using fluorescence spectroscopy. The changes in the emission maxima of Nile Red were plotted as a function of the mole fraction of the less polar solvent. The systems behaved nonideally. This nonideality was explained by dielectric enrichment and by hydrogen bonding.

Chapter 4

SOLUBILITY OF L-LYSINE MONOHYDROCHLORIDE

4.1 Introduction

No published solubility data were found for l-lysine monohydrochloride. Therefore, the solubility data for l-lysine monohydrochloride in two solvents, water and ethanol, was determined within a narrow temperature range. The solubility in mixtures of water and ethanol will also be presented. Furthermore, the implications of these data on the purification of l-lysine monohydrochloride by recrystallization will be addressed.

Orella and Kirwan [42] have studied various other amino acids. Their results were presented in Chapter 1 (Figure 1.4). They reported that adding alcohol to aqueous amino acid mixtures can have a significant effect on the solubility. They have concluded that the effect depends on the polarity of the side chains of the amino acid. From the previous chapter it can be seen that adding ethanol to water affects the polarity of the system greatly. Thus, the l-lysine monohydrochloride solubility would also be expected to decrease dramatically.

This chapter is based on parts of a manuscript titled "*In situ* monitoring of antisolvent crystallization using attenuated total reflection Fourier transform infrared spectroscopy" by Uusi-Penttilä and Berglund [55].

4.2 Solubility of l-lysine monohydrochloride in water

The solubility of l-lysine monohydrochloride in water as a function of temperature was determined first. The procedure for solubility measurement was taken from Myerson and Ginde [38]. Distilled water and an excess amount of l-lysine monohydrochloride were stirred in a temperature controlled sealed vessel for 24 hours. The solids were filtered, dried and weighted, and the equilibrium concentration of l-lysine monohydrochloride was calculated. This procedure was repeated for different temperatures and a solubility curve was obtained for a narrow temperature range and is presented in Figure 4.1.

$$w_{limhc} = 0.46\ T + 29.6 \qquad (20\ °C \le T \le 45\ °C) \qquad 4.1$$

where w_{limhc} is w-% of l-lysine monohydrochloride, and T is temperature.

As can be seen from Figure 4.1, the l-lysine monohydrochloride solubility in water is only slightly dependent on the temperature. Within a range of 25 °C (from 20 °C to 45 °C) the solubility increases only from about 40 weight-% up to about 50 weight-%. In cooling crystallization, therefore, the yield of l-lysine monohydrochloride would be very small.

4.3 Solubility of l-lysine monohydrochloride in ethanol

Similar control experiments were done to determine l-lysine monohydrochloride solubility in ethanol. Within the temperature range from 15 °C to 50 °C the solubility varied between 0 and 2 weight-%. Therefore, the l-lysine monohydrochloride solubility in ethanol was assumed to be negligible in the crystallization experiments.

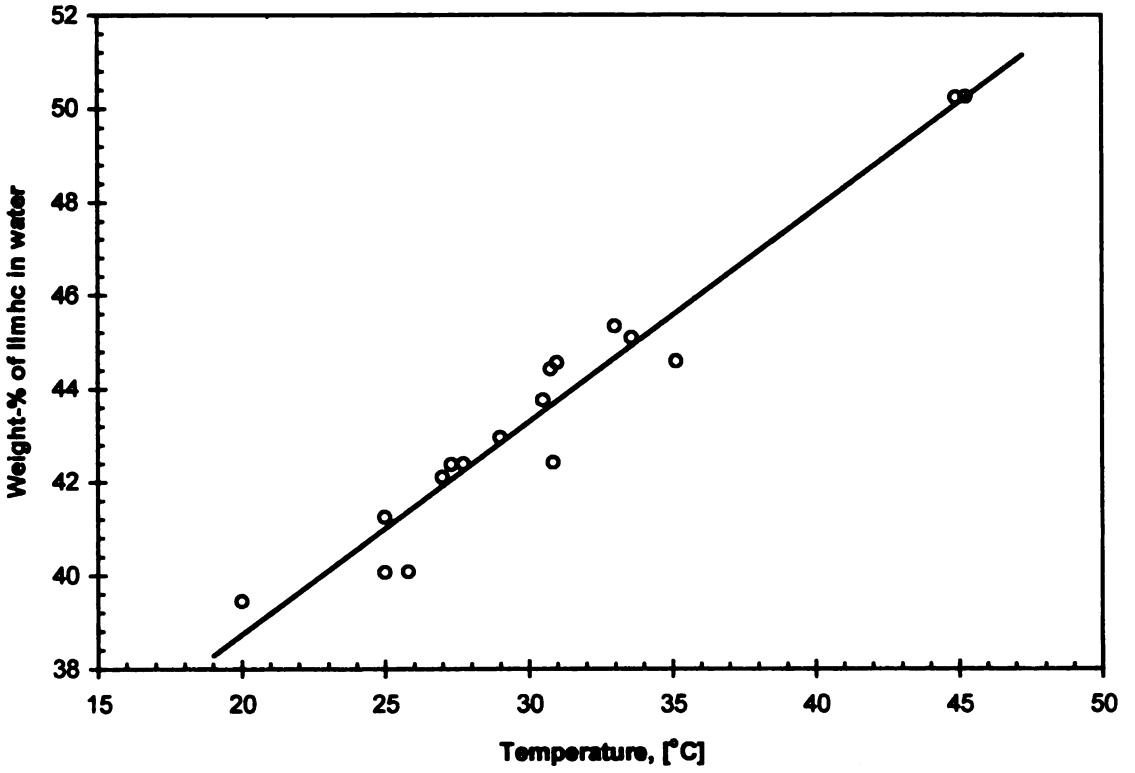

Figure 4.1. Solubility of l-lysine monohydrochloride in water as a function of temperature.

4.4 Solubility of l-lysine monohydrochloride in ethanol-water mixtures

The previous procedure was also used for ternary l-lysine monohydrochloride-ethanol-water systems. The solubility of l-lysine monohydrochloride in various binary mixtures of water and ethanol was determined at 303 ± 1 K. Figure 4.2 shows the solubility curve. During the actual antisolvent crystallization experiments the amount of water in the crystallizer was chosen to be kept constant. Therefore, this solubility curve was normalized based on the amount of water in the crystallizer. The following equation was fitted from the experimental data:

$$\frac{m_L}{m_w} = \frac{0.33}{0.44 + \frac{m_e}{m_w}} - 0.02 \qquad 4.2$$

where m_L is the mass of l-lysine monohydrochloride, m_w is the mass of water, and m_e is the mass of ethanol.

4.5 Discussion

Figure 4.1 shows that l-lysine monohydrochloride solubility in water is not very temperature sensitive. Therefore, a cooling crystallization is not efficient for l-lysine monohydrochloride purification. It should also be noted that an amino acid should not be exposed to very high temperatures. However, based on the large decrease of the l-lysine monohydrochloride solubility in the presence of ethanol, an alternative method for l-lysine monohydrochloride purification is proposed: antisolvent crystallization. This method easily produces yields of 90 w-%. The other advantage is the possibility of doing the crystallization at a low temperature.

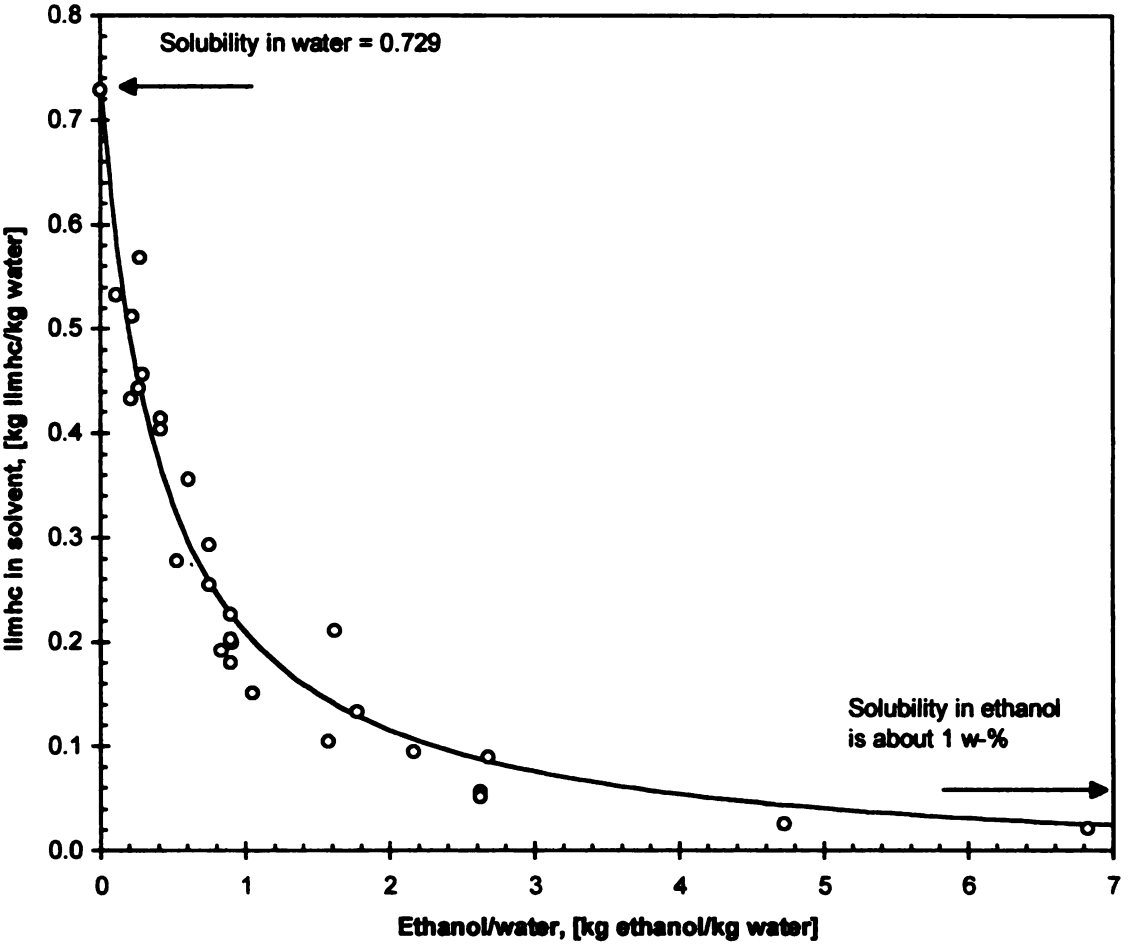

Figure 4.2. Solubility of l-lysine monohydrochloride in various binary mixtures of water and ethanol at 303 ± 1 K.

4.6 Conclusions

Solubility data for l-lysine monohydrochloride in water, in ethanol, and in mixtures of ethanol and water were determined. It was concluded that due to the minimal temperature dependence of l-lysine monohydrochloride solubility in water, cooling crystallization is not an effective way to purify l-lysine monohydrochloride. However, adding ethanol into an l-lysine monohydrochloride-water system decreases the solubility of l-lysine monohydrochloride in water significantly. This effect can be exploited in the purification of l-lysine monohydrochloride.

Chapter 5

IN SITU MONITORING OF ETHANOL AND L-LYSINE MONOHYDROCHLORIDE CONCENTRATION IN A BENCH SCALE CRYSTALLIZER WITH ATR FTIR

5.1 Introduction

Antisolvent crystallization is a commonly used crystallization method in pharmaceutical industry. Therefore, purification of l-lysine monohydrochloride using ethanol as an antisolvent was chosen to simulate a pharmaceutical crystallization process. The process was monitored using attenuated total reflection Fourier transform infrared (ATR FTIR) spectroscopy. The unique configuration of the DIPPER® 210 deep immersion probe made it possible to monitor the liquid phase *in situ* in the crystallizer. The applicability of this method for monitoring batch cooling crystallization has been demonstrated by Dunuwila et al. [13] and by Dunuwila [12]. However, the peak shift approach that they used was not applicable for this system. Therefore, the infrared peak intensity changes were used to monitor the system.

This chapter presents the calibration curves that correlate component concentrations with infrared peak intensities. The infrared spectrum of a three component system is very complex. Some of the characteristic peaks for the solute, solvent and antisolvent are so close to each other that they appear as one peak in the infrared spectrum. Therefore, derivative spectroscopy was used to resolve the overlapping infrared peaks into the individual component peaks. Special care was taken to find peaks that are not influenced by the other components in the crystallizer.

This chapter is based on parts of a manuscript titled "*In situ* monitoring of antisolvent crystallization using attenuated total reflection Fourier transform infrared spectroscopy" by Uusi-Penttilä and Berglund [55].

5.2 Experimental

5.2.1 Materials

The antisolvent crystallization system of choice for the current experiments was recrystallization of l-lysine monohydrochloride. The solvent was water and the antisolvent was ethanol. L-lysine monohydrochloride (USP grade) was purchased from Kyowa Hakko Kogyo Company. Ethanol (anhydrous) was obtained from Quantum Chemical Corporation. Distilled water was used in all experiments. The ethanol was used without further purification and l-lysine monohydrochloride was recrystallized before use.

5.2.2 Instrumentation

A one liter, jacketed crystallizer is kept at a constant temperature (30 °C) for the calibration measurements. The spectrometer is a Perkin-Elmer 1750 Fourier transform infrared spectrometer, and the ATR element used is a DIPPER® 210 deep immersion probe with an AMTIR® ATR crystal from Axiom Analytical.

5.3 Attenuated total reflection Fourier transform infrared spectroscopy

5.3.1 Introduction to ATR FTIR spectroscopy

In attenuated total reflection Fourier transform infrared (ATR FTIR) spectroscopy the infrared radiation is directed into the interface between the reflectance element and the sample in such an angle that all the radiation is reflected back. In order for this to be possible, the reflectance element has to be of optically denser material than the sample is, and the incident angle of the infrared radiation has to be larger than the ratio of the refractive index of the sample over the refractive index of the reflectance element. According to Colthup [9] and Mirabella [32], despite the total reflection of the radiation at the interface, there is an evanescent wave that persists into the sample as illustrated in Figure 5.1.

Two most common variables measured with infrared spectroscopy are the transmittance, T, and the absorbance, A [19].

$$T = 10^{-abc} \qquad 5.1$$

and

$$A = -\log T = abc \qquad 5.2$$

where a is absorptivity, b is pathlength, and c is concentration.

In attenuated total reflection spectroscopy an effective pathlength is used. This pathlength is defined as the product of the number of reflection points in contact with the sample on the surface of the reflection element, N, and the depth of penetration, d_p, (Coetzee [8]).

$$b = N d_p \qquad 5.3$$

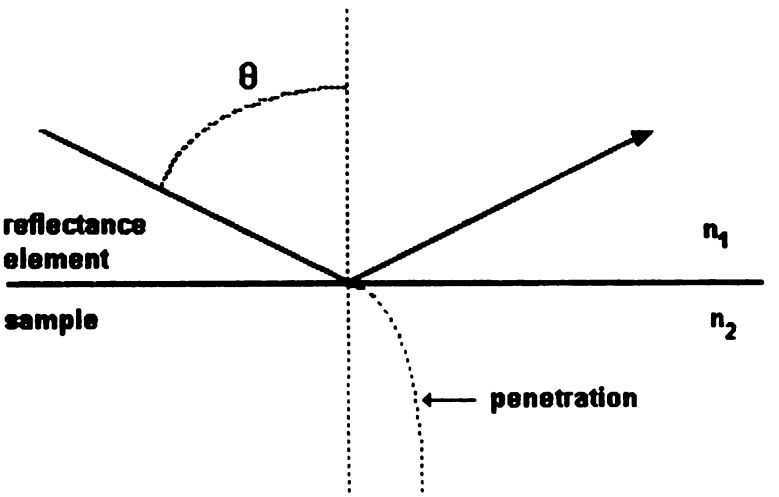

Figure 5.1. Total internal reflection.

The wavelength dependent penetration depth of the evanescent wave is obtained according to Ingle and Crouch [19] and Müller and Abraham-Fuchs [33] from

$$d_p = \frac{\lambda_c}{\left\{2\pi\left[\sin^2\theta - \left(\eta_s / \eta_c\right)^2\right]\right\}^{1/2}} \qquad 5.4$$

where λ_c is the wavelength in the ATR crystal, θ is the incident angle of the infrared radiation, η_s is the refrective index of sample, and η_c is the refractive index of the ATR crystal.

The penetration depth as a function of the wavelength for both pure water and pure ethanol was calculated using Equation 5.4. The results are presented in Figure 5.2. It can be seen that there is hardly any difference from solvent to solvent. Therefore, the differences in the spectra cannot be attributed to the change in the penetration depth because of the change of solvent. Also, the penetration depth is so small that there is no interference from the crystals. Therefore, it can be safely assumed that the spectrum reflects the liquid phase conditions. This attribute is why this method is excellent also for heavy slurries.

According to Colthup [9] and Mirabella [32], the evanescent wave has the same wavelength as the infrared radiation and decays exponentially in the optically less dense medium. The wave interacts with the reflected radiation at the interface by either reducing it or increasing it, and thus, producing an infrared spectrum of the sample. Figure 5.3 shows the transmission spectra for ethanol, water and aqueous l-lysine monohydrochloride.

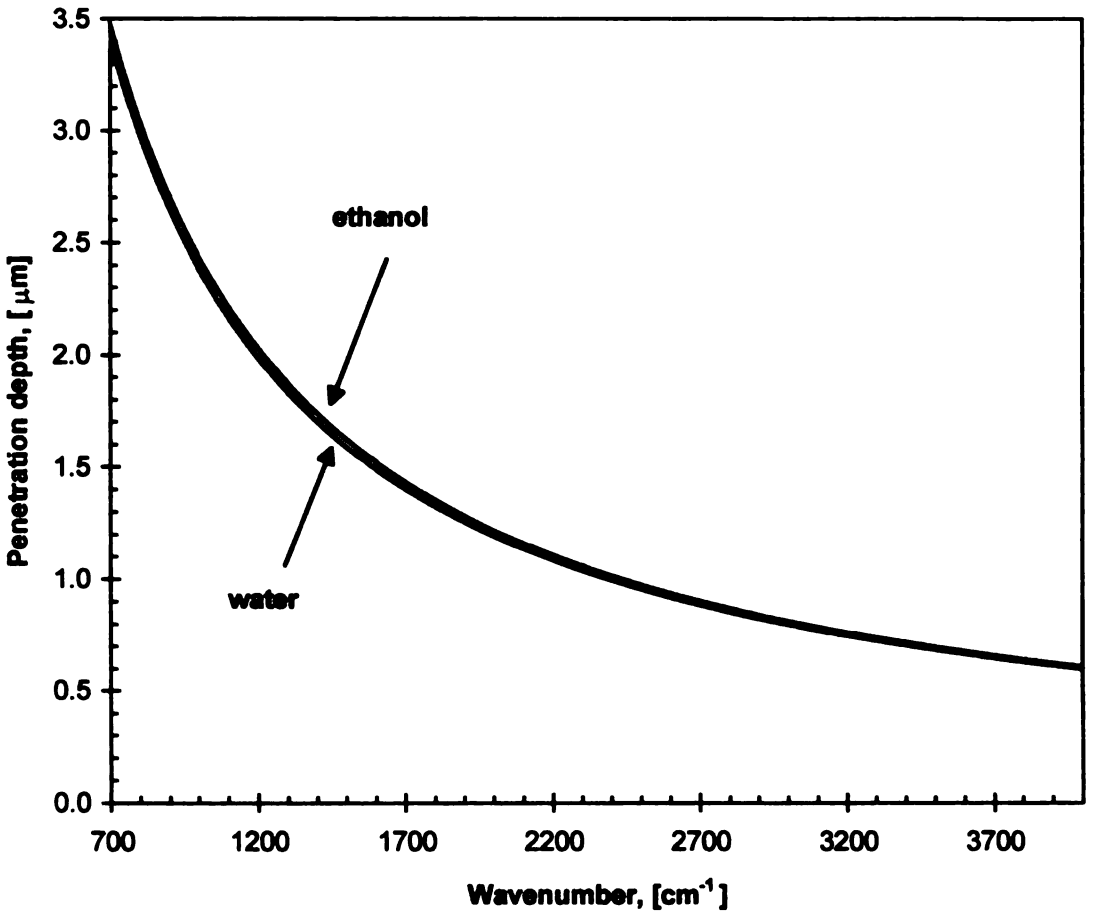

Figure 5.2. Penetration depth of the evanescent wave for pure water and pure ethanol as a function of wavenumber.

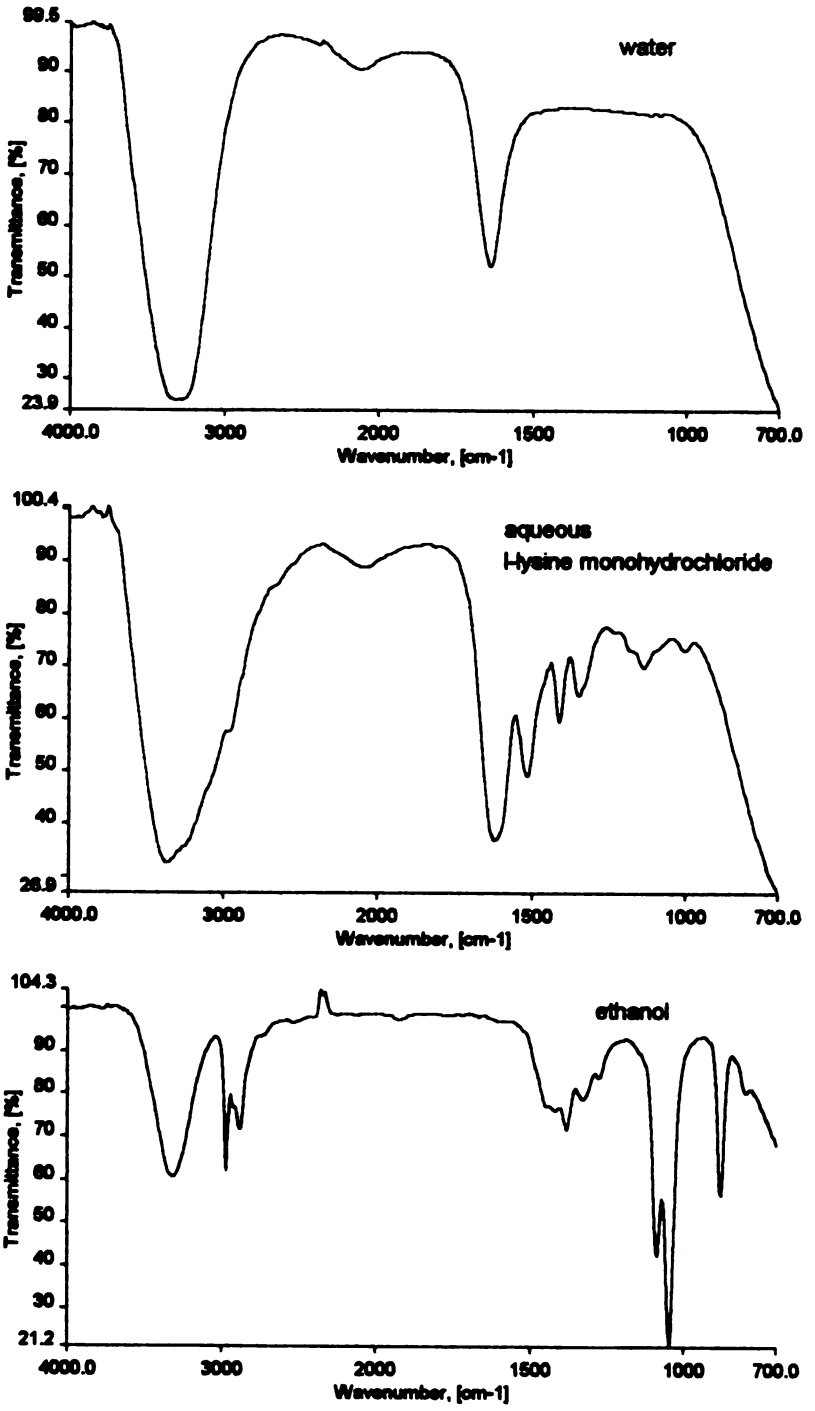

Figure 5.3. Infrared spectra of water, aqueous l-lysine monohydrochloride, and ethanol at 30 °C.

5.3.2 Derivative spectroscopy

It can be seen from Figure 5.3 that several of the peaks within the region from 1300 cm^{-1} to 1700 cm^{-1} are overlapping. The ethanol peaks at 1042 cm^{-1} or 1088 cm^{-1} can be used to determine the ethanol concentration. To determine the l-lysine monohydrochloride concentration in the solution the overlapping peaks have to be resolved. Derivative spectroscopy was used.

Derivative spectroscopy enhances the fine structures of the spectrum [5], [6], [18], [27], [28]. For two peaks that are so close to each other that they appear as one peak in the infrared spectrum, the second derivative of the spectrum can be used to resolve these peaks into two separate peaks. Figure 5.4 demonstrates this. The first derivative crosses the zero baseline at the position of the peak maximum of the original spectrum. The second derivative has a minimum at the peak position.

Cahill [5, 6] points out that due to the linear nature of derivation operation, the peak intensities of the second derivative spectrum follow Beer's law just like the intensities of the original spectrum. Therefore, the peak intensities of the second derivative spectra can be used to determine the solution concentrations. The main problem with this data treatment method is the fact that the signal-to-noise ratio has to be low for this method to work.

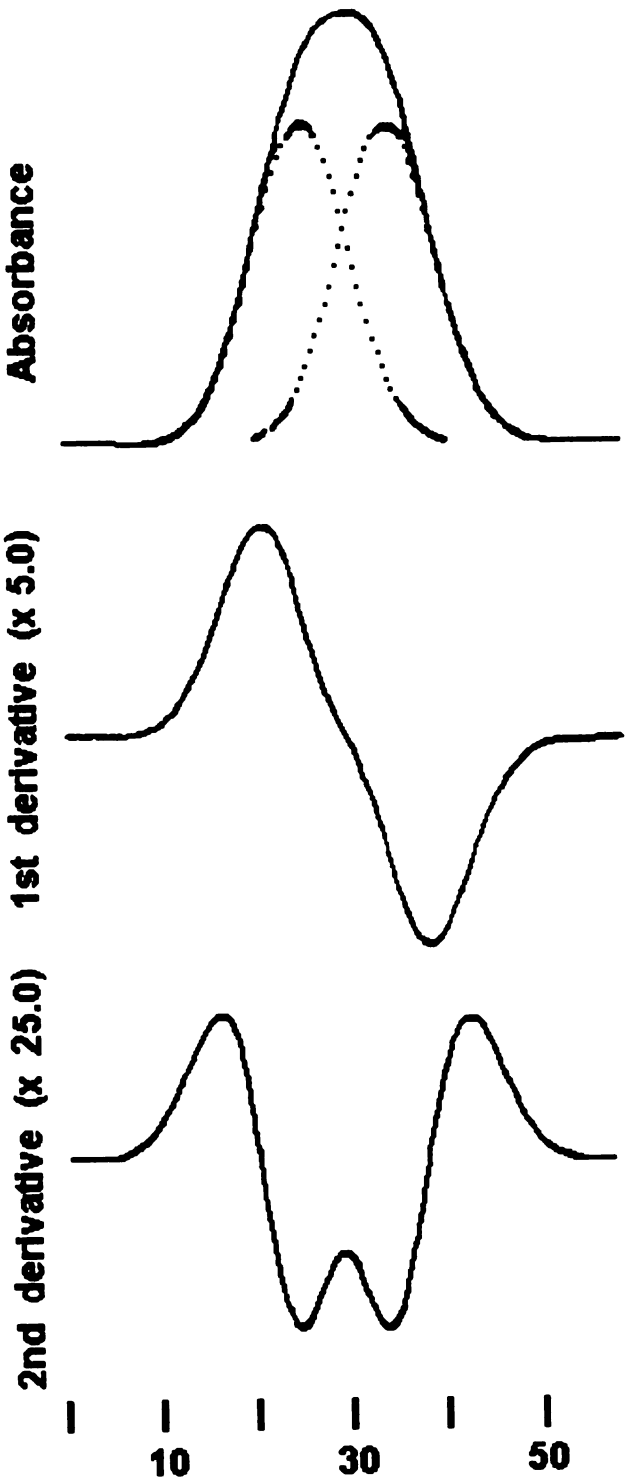

Figure 5.4. First and second derivatives for two overlapping Gaussian bands (Cahill [5]).

5.4 Calibration of infrared spectra and component concentrations

5.4.1 Calibration curve for ethanol concentration

Figure 5.3 showed the transmission spectra of the pure components in the crystallizer. Either one of the two main peaks in the ethanol spectrum, i.e. 1042 cm^{-1} or 1088 cm^{-1}, can be used to determine the ethanol concentration. Because of the better sensitivity the C-O stretching vibration peak at 1042 cm^{-1} is chosen. Using Equation 5.2 the transmission spectrum was changed into an absorption spectrum and the ethanol concentration was calculated.

To prevent disturbance due to baseline fluctuations from experiment to experiment, a relative absorbance A_r is preferred. Therefore, the following formula is used to relate the ethanol concentration and the infrared measurement

$$A_r = A_{1042} / A_{1110} \qquad 5.5$$

where A_{1042} is the absorbance at 1042 cm^{-1}, and A_{1110} is the absorbance at 1110 cm^{-1}.

The calibration curve for ethanol concentration is presented in Figure 5.5. In the crystallization experiments, the amount of ethanol varies between 0 and 61 w-%. Therefore, a linear correlation is used for the relative absorbance and the mass of ethanol.

$$A_r = 1 - 0.32 \frac{m_e}{m_e + m_w} \qquad 5.6$$

or solving for the mass of ethanol

$$m_e = \frac{(1 - A_r)\, m_w}{A_r - 0.69} \qquad 5.7$$

where m_e is the mass of ethanol, and m_w is the mass of water.

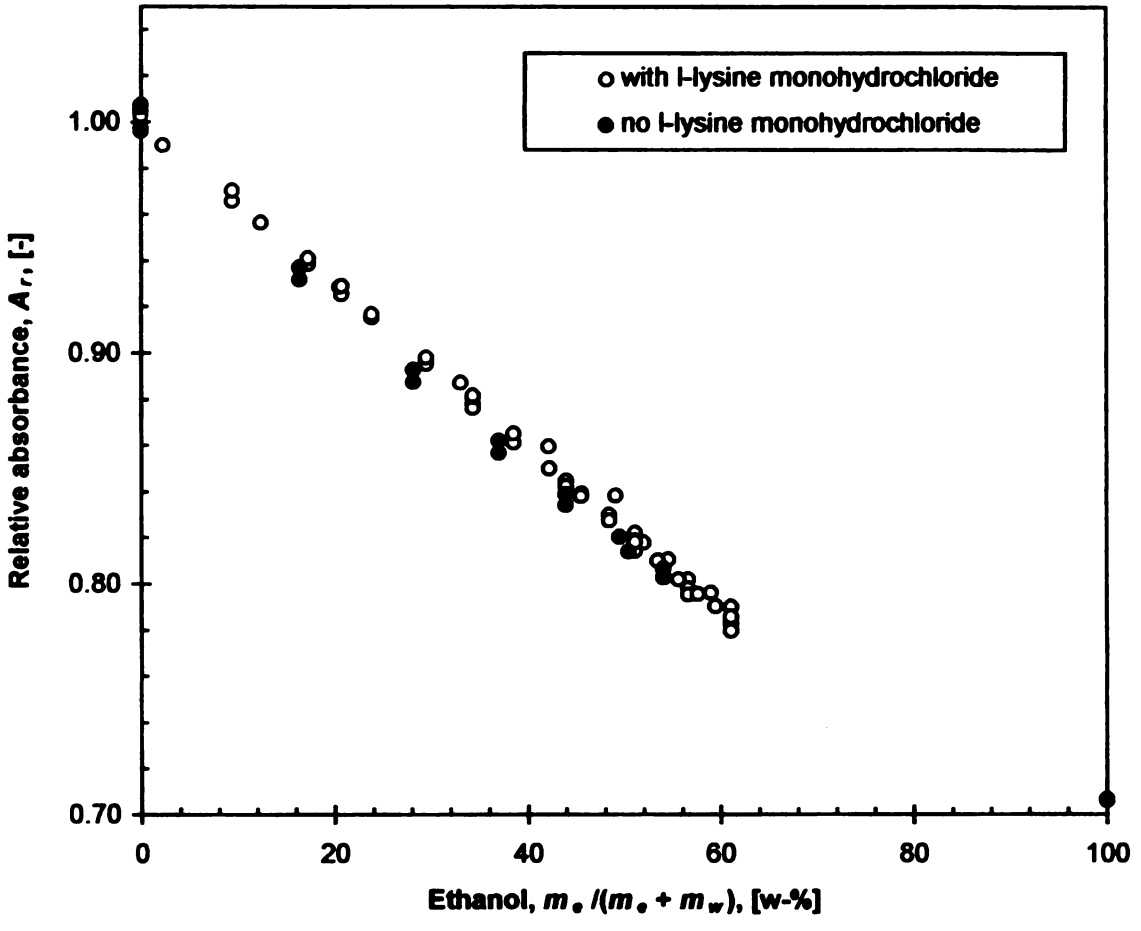

Figure 5.5. Relative absorbance, A_r, as a function of ethanol weight percentage.

5.4.2 Calibration curve for l-lysine monohydrochloride concentration

The determination of the concentration of l-lysine monohydrochloride is more complicated. L-lysine monohydrochloride has a variety of functional groups available. However, as can be seen from Figure 5.3, the l-lysine monohydrochloride peaks fall in the same region as peaks from ethanol. To overcome this problem derivative spectroscopy was chosen to resolve the overlapping peaks.

For accurate solute concentration measurements it is important to find a peak that is not affected by the presence of the two solvents. The second derivative spectrum of l-lysine monohydrochloride was studied, and a carboxylate band at 1411 cm^{-1} was not affected by the presence of ethanol. This was verified using multivariate analysis. The correlations between the band at 1411 cm^{-1}, l-lysine monohydrochloride concentration and ethanol concentration were calculated. The correlation coefficients are shown in Table 5.1. It is clear that there is no correlation between the ethanol concentration and the band at 1411 cm^{-1}. Therefore, this peak was chosen for the determination of the l-lysine monohydrochloride concentration in the crystallizer.

Table 5.1. Correlation coefficients for multivariate analysis of the band at 1411 cm^{-1}, l-lysine monohydrochloride concentration and ethanol concentration.

Ethanol concentration and l-lysine monohydrochloride concentration	Ethanol concentration and the band 1411 cm^{-1}	L-lysine monohydrochloride concentration and the band 1411 cm^{-1}
-0.51	-0.48	0.93

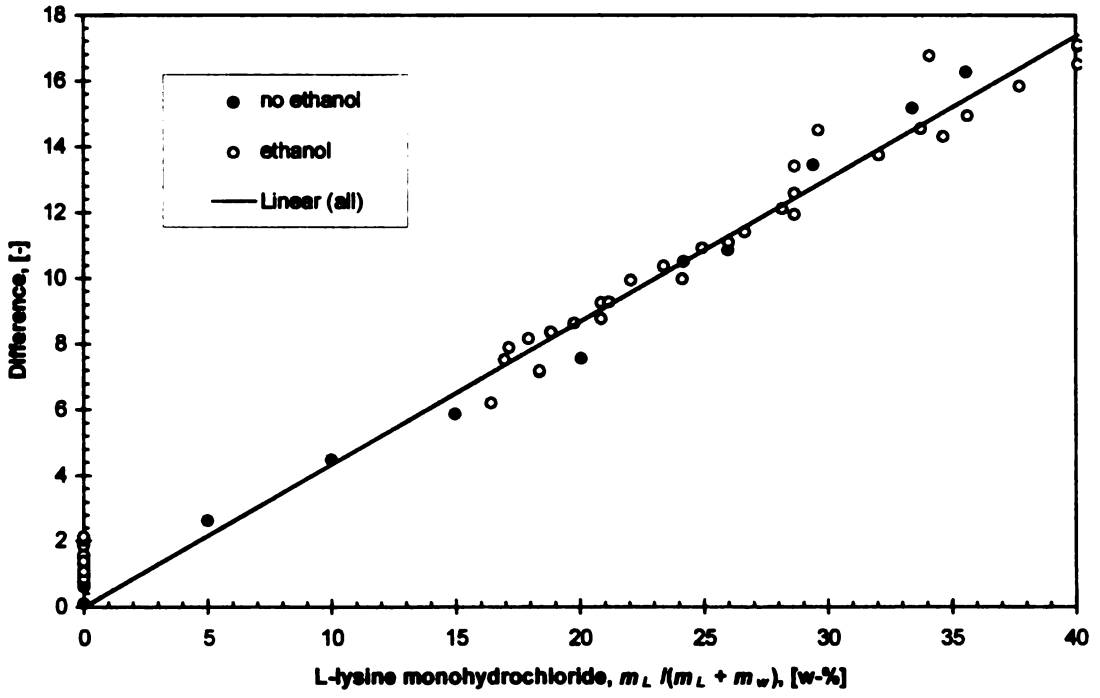

Figure 5.6. Difference of the second derivative peaks at 1411 cm^{-1} and 1432 cm^{-1} as a function of the weight fraction of l-lysine monohydrochloride.

To eliminate the baseline fluctuations the following difference, D, was used for the calibration

$$D = I_{1411} - I_{1432} \qquad 5.8$$

where I_{1411} is the intensity of the second derivative at 1411 cm^{-1}, and I_{1432} is the intensity of the second derivative at 1432 cm^{-1}.

Figure 5.6 shows the calibration curve for l-lysine monohydrochloride concentration. The following correlation can be obtained for the difference and l-lysine monohydrochloride

$$D = 43.4 \frac{m_L}{(m_L + m_e + m_w)} \qquad 5.9$$

and solving for the amount of l-lysine monohydrochloride

$$m_L = \frac{D(m_e + m_w)}{43.4 - D} \qquad 5.10$$

where m_L is the mass of l-lysine monohydrochloride, m_e is the mass of ethanol, and m_w is the mass of water.

5.5 Conclusions

In this chapter the calibration curves for ethanol concentration and l-lysine monohydrochloride concentration and infrared spectra were generated. Derivative spectroscopy was used to calibrate l-lysine monohydrochloride concentration. Within the operating range both calibration curves can be fitted to a linear approximation. These curves were used in Chapters 7 and 8 to determine the effect of the antisolvent addition rate on various parameters.

Chapter 6

EXPERIMENTAL ARRANGEMENT AND CRYSTALLIZATION PROCEDURE

6.1 Introduction

This chapter shows the experimental arrangement for monitoring the purification of l-lysine monohydrochloride using attenuated total reflection Fourier transform infrared spectroscopy. The procedure for the crystallization and the product treatment will also be explained.

6.2. Materials

The antisolvent crystallization system of choice for the current experiments was recrystallization of l-lysine monohydrochloride. The solvent was water and the antisolvent was ethanol. L-lysine monohydrochloride (USP grade) was purchased from Kyowa Hakko Kogyo Company. Ethanol (anhydrous) was bought from Quantum Chemical Corporation. Distilled water was used in all experiments. The ethanol was used without further purification. The crystallized l-lysine monohydrochloride was reused in the next batches.

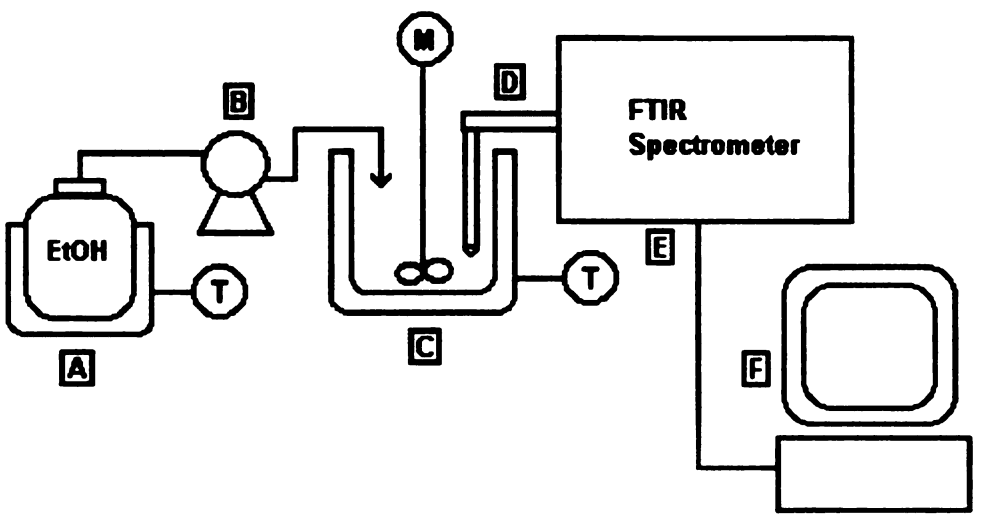

Figure 6.1. The experimental arrangement: **A** temperature controlled antisolvent reservoir; **B** pump; **C** jacketed crystallizer with a marine type impeller; **D** Dipper-210 deep immersion probe; **E** FTIR spectrometer; **F** computer.

6.3 Instrumentation

Figure 6.1 shows the experimental arrangement. A one liter, jacketed crystallizer is used for the crystallization. It is kept at a constant temperature (30 ± 1 °C) with Brinkmann's RC6 LAUDA water bath. The crystallizer is equipped with a marine type impeller.

The antisolvent reservoir is placed in a waterbath and kept at the same temperature as the crystallizer. A peristaltic pump is used to add the antisolvent at rates of 5 ml/min or more. A syringe pump is used for smaller addition rates. The capacity of the syringe pump was one fifth of the total amount of the added antisolvent. Therefore, for the small addition rates the antisolvent addition had to be stopped momentarily five times during the crystallization to fill up the syringe. This did not have significant effect on the results.

The spectrometer is a Perkin-Elmer 1750 Fourier transform infrared spectrometer. The ATR element is a DIPPER® 210 deep immersion probe with an AMTIR® ATR crystal by Axiom Analytical [1]. AMTIR® is a mixture of Arsenic, Selenium and Germanium glass. Its refractive index is 2.5 at 1000 cm^{-1}, and the spectral range is 11,000-750 cm^{-1} [7]. The DIPPER® 210 is dipped straight into the solution in the crystallizer and a program is run to take the spectra of the solution at desired time intervals.

6.4 Crystallization

The crystallization is started by preparing a saturated aqueous l-lysine monohydrochloride solution at 30 °C. From Chapter 4, the solubility of l-lysine monohydrochloride at 30 °C is 42 w-%, is equivalent to 109 g of l-lysine monohydrochloride and 150 ml of distilled water. Ethanol at 30 °C is added at a constant addition rate using either a peristaltic pump or a syringe

pump. To obtain good yields the crystallization is continued until 300 ml of ethanol has been added.

The product is filtered using a water jet pump. The filter used is a Lab Glass fritted disc funnel with a pore size of 10-15 μm. The crystals are washed twice with 150 ml of ethanol and dried in an oven overnight at 50 °C.

6.5 Sieving

The crystal size distribution of the dried product is determined by sieving. The procedure for the sieving and the length of the sieving time are according to Irani and Callis [20] and ASTM Standard No. 447B [29]. The sieving time is long enough when the weight of the sieve fraction on a sieve during the sieving does not change more than 1 w-% within the specified period of time.

The crystals are sieved using two sets of sieves. First, the larger particle sizes (> 0.425 mm) are divided into eight sieve cuts. The adequate time is 25 minutes using a W.S. Tyler Model RX-86 sieve shaker and a W.S. Tyler (20 cm diameter) sieve set. The bottom fraction (< 0.425 mm) is sieved for another 20 minutes using a Scientific Industries Vortex-Genie 2 shaker and W.S. Tyler (5 cm diameter) sieve set. This arrangement divides the product further into six fractions. The sieve cuts for the sieve series are presented in Table 6.1.

Table 6.1. Two sieve series used for determining the product crystal size distribution.

20 cm diameter sieves	5 cm diameter sieves
1.18 mm	0.355 mm
1.00 mm	0.250 mm
0.85 mm	0.180 mm
0.71 mm	0.125 mm
0.60 mm	0.090 mm
0.50 mm	
0.425 mm	

Chapter 7

L-LYSINE MONOHYDROCHLORIDE KINETICS

7.1 Introduction

Determining the growth and nucleation kinetics for a batch experiment is tedious and time consuming. Usually this is done from continuous experiments. The most common correlations used for growth and nucleation kinetics are empirical power-law expressions (Wey [59]).

$$G = k_g \Delta c^g \qquad 7.1$$

$$B_o = k_N \Delta c^b (m_T)^j \qquad 7.2$$

where G is the growth rate, k_g is the growth rate constant, Δc is the supersaturation, g is the growth order, B_o is the nucleation rate, k_N is the nucleation rate constant, b is the nucleation kinetic order, m_T is the suspension density, and j is the exponent of suspension density.

This chapter shows the results of nucleation cell experiments. These experiments were used to determine whether the growth rate of an individual l-lysine monohydrochloride crystal is size-dependent or size-independent. Then seeded experiments were used to estimate the overall growth rate in the crystallizer. Finally, the nucleation rates were iterated from the population balance using the moment equations.

7.2 Crystal growth

7.2.1 Growth rate dependency on crystal size

Two sets of nucleation cell experiments were conducted to determine whether the growth rate of l-lysine monohydrochloride crystals is size-dependent or not. The first set of experiments was done using only water as the solvent, and the second set of experiments had a mixture of water and ethanol as the solvent. The experimental arrangement is from Shanks and Berglund [46] as presented in Figure 7.1. The nucleation cell is temperature controlled at 30 ± 1 °C.

A supersaturated solution of l-lysine monohydrochloride is made by adding an excess amount of l-lysine monohydrochloride into the solvent in a beaker. The solution is heated until all l-lysine monohydrochloride is dissolved, and then cooled slowly down to 30 °C. The nucleation cell is filled with supersaturated solution. A parent crystal that has been glued to a rod is placed into the supersaturated solution. The nucleation cell is closed and the parent crystal is dragged over a glass plate. This causes nucleation. The growth of nuclei is followed by taking photographs of the nucleation cell through a microscope. The growth rate of the l-lysine monohydrochloride crystals is then determined from the photographs.

To determine the growth rate of the crystals a spherical equivalent diameter was used.

$$A_{eq} = w\,l = \pi r^2 \qquad 7.3$$

where A_{eq} is the area of the rectangular crystal and a sphere of an equal size, w is the width of the crystal, l is the length of the crystal, and r is the radius of a sphere.

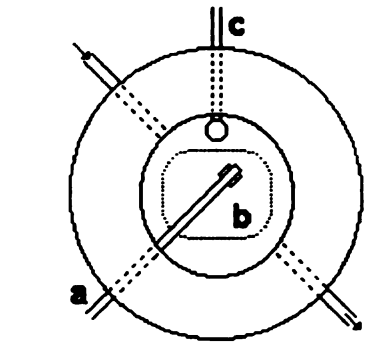

top view

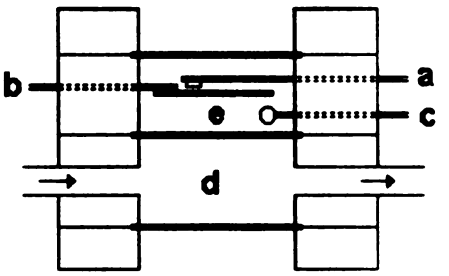

side view

Figure 7.1. The temperature controlled nucleation cell. **a** rod with parent crystal glued to it, **b** glass slide and the rod it is glued to, **c** temperature element, **d** chamber for constant temperature water, **e** chamber for saturated solution. [46]

This equation is solved for the radius of the sphere, r, which is taken as size of the crystal. Figure 7.2 shows the spherical equivalent size of the crystals grown in the nucleation cell experiments as a function of time. For the ethanol-water experiments nine different crystals from three experiments were measured, and for the water experiments eleven crystals from two experiments were measured. All the measured crystals follow a linear trend. The slope of this trend is the growth rate. Figure 7.2 also clearly demonstrates that there is no difference in the individual growth rates from one experiment to the other. Therefore, the presence of ethanol does not seem to effect the growth kinetics significantly. Also, since the slope is constant, the growth rate of l-lysine monohydrochloride crystals is size-independent.

7.2.2 Overall growth rate from seeded experiments

The overall growth rate for the l-lysine monohydrochloride crystals in the batch experiments was estimated from nine seeded experiments. The crystallizations were run at three different lengths of time for three different antisolvent addition rates. Figure 7.3 shows the actual crystal mass retained on each sieve at 20 ml/min ethanol addition rate after 2, 5, and 10 minutes of crystallization. The sieve cuts that were smaller than 550 μm were ignored and the weight mean size of the grown seed crystals was determined using the following equation.

$$L_{wm} = \Sigma(L_i w_i) / \Sigma w_i \qquad 7.4$$

where L_i is the mean size of a sieve cut i in μm, and w_i is the mass of crystals on sieve i in grams.

The weight mean sizes were plotted as a function of time and the following overall growth rates were obtained: 7.1 μm/min for 1 ml/min ethanol addition rate, 10 μm/min for 5 ml/min, and

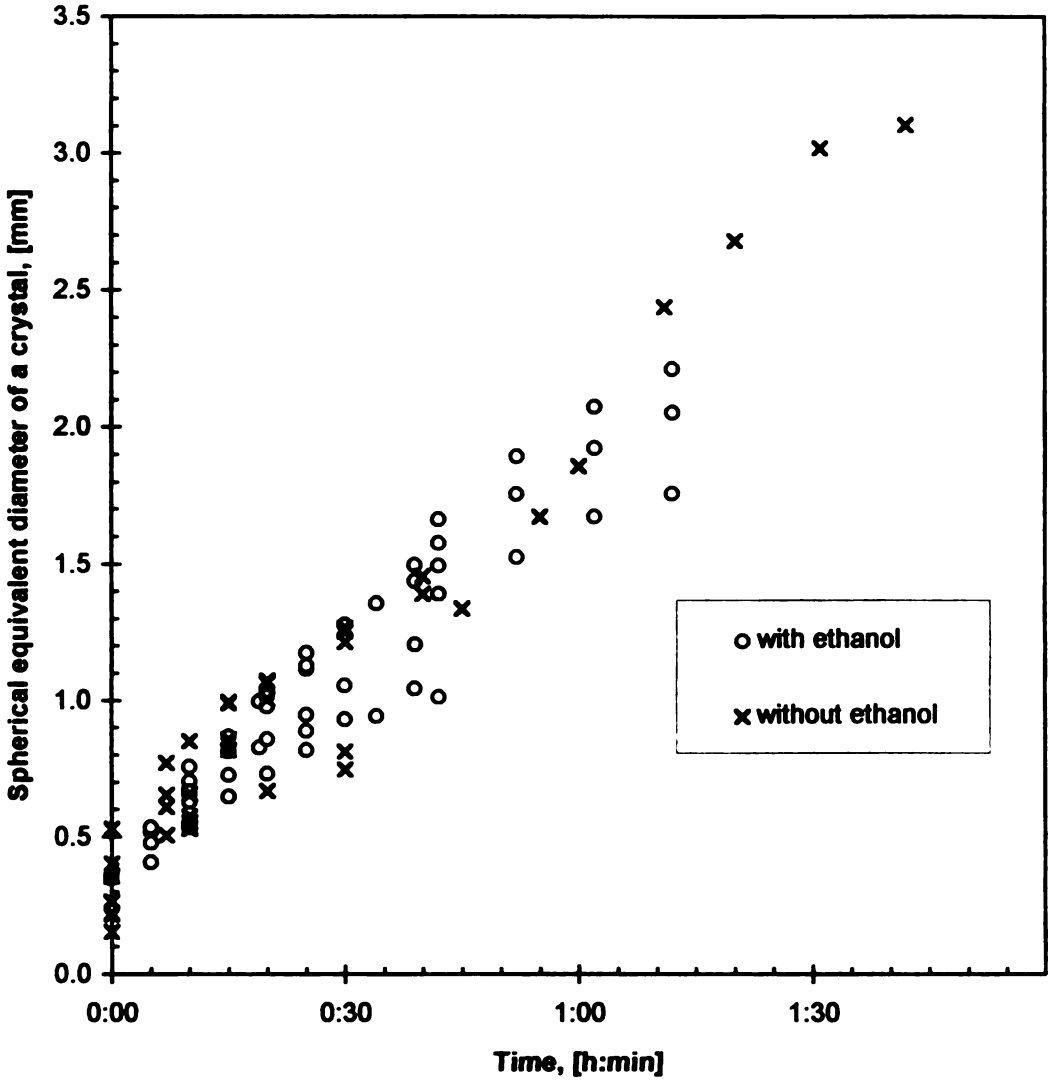

Figure 7.2. Spherical equivalent diameter for single crystals in a seeded nucleation cell. The experiments were done at 30 °C and the ethanol/water ratio was 1.2:1 on volume basis.

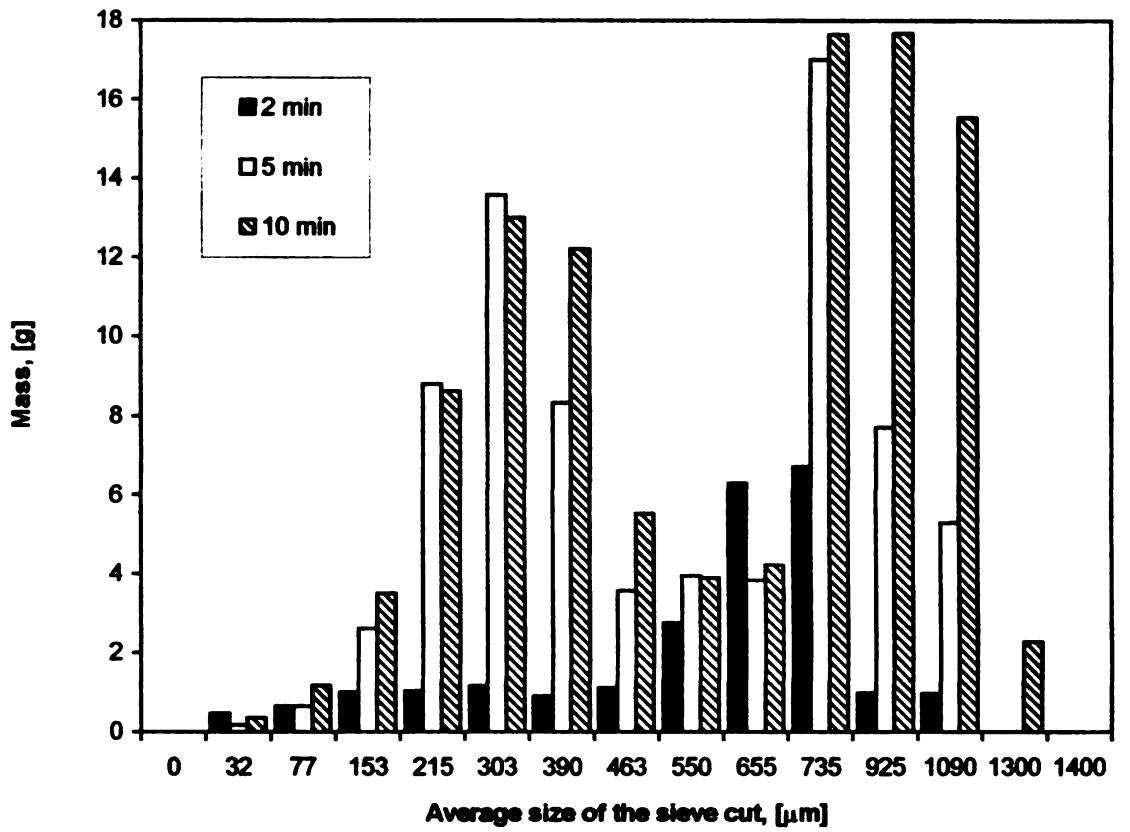

Figure 7.3. Mass of l-lysine monohydrochloride crystals retained on the sieves after 2, 5, and 10 minutes of crystallization. The experiment was done at 30 °C and the ethanol addition rate was 20 ml/min. The average seed size was 550 μm and the mass of seeds was 10 g.

31 μm/min for 20 ml/min addition. These rates are plotted in Figure 7.4 and the following estimate for the overall growth rate as a function of ethanol addition rate is obtained

$$G = 1.28 * Q_e + 4.9 \qquad 7.5$$

where the growth rate, G, is expressed in μm/min, and ethanol addition rate, Q_e, in ml/min.

As will be shown in Chapter 8, in the antisolvent crystallization of l-lysine monohydrochloride the supersaturation is only a function of the concentration of ethanol in the crystallizer. Rather than presenting the growth rate as a function of supersaturation, all the constants and the variables that depend on the ethanol addition rate are grouped together. Thus, the overall growth rate is presented as a function of the ethanol addition rate only.

7.3 Nucleation

To estimate the nucleation rate for the l-lysine monohydrochloride purification, the crystal size distributions from the seeded experiments were compared with the unseeded experiments. Figure 7.5 shows the difference in the mass of nuclei in the seeded experiments and unseeded experiments. It can be seen that the amount of small crystals is significantly smaller in seeded experiments. This smaller amount can be attributed to Ostwald ripening. In that, particles in a suspension with different particle sizes dissolve at different speeds depending on the particle size. The small particles dissolve and deposit on the bigger particles. This preferential dissolution decreases the amount of fines in the product and increases the average crystal size of the product (Myerson [36]). Thus, the nucleation rate is estimated from unseeded experiments.

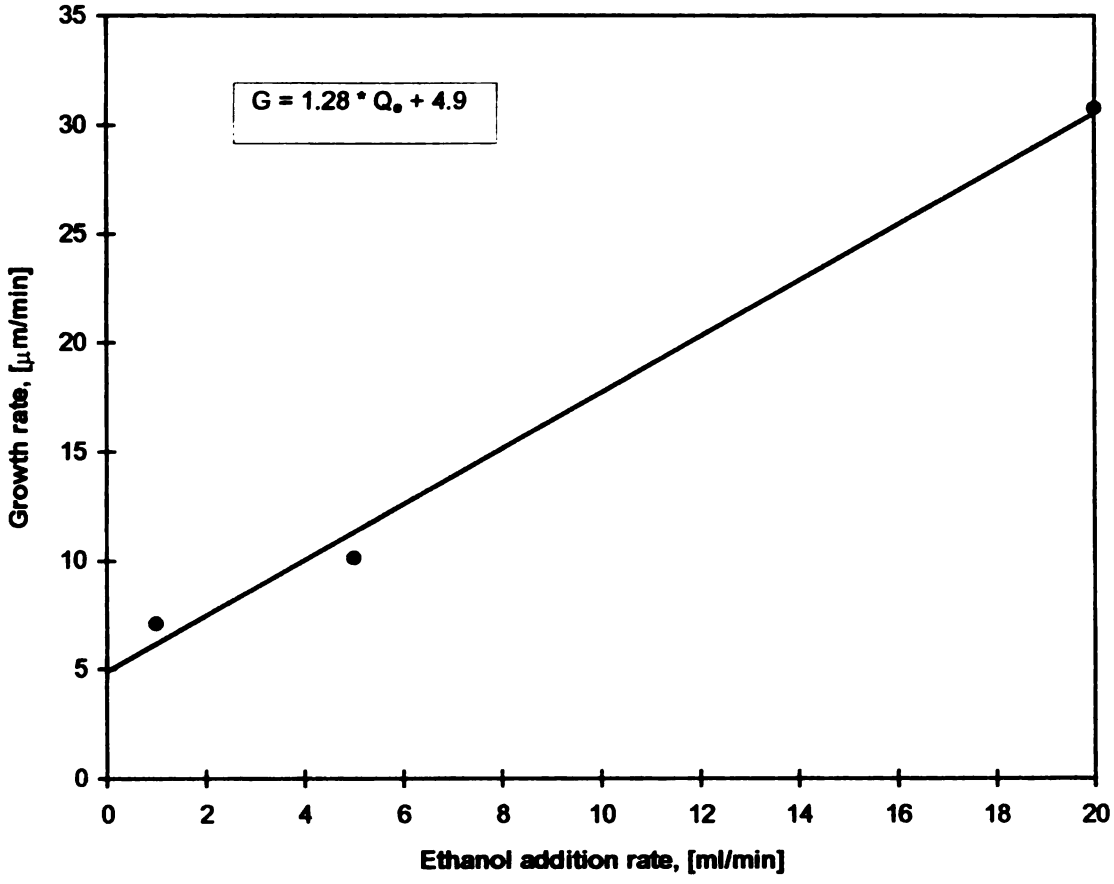

Figure 7.4. Estimate for the overall growth rate of l-lysine monohydrochloride as a function of ethanol addition rate from seeded experiments.

Using the previously obtained overall growth rate and experimental suspension density, the nucleation rate can be estimated from the population balance [44], [59]

$$\frac{\partial(nV)}{\partial t} + \frac{\partial(GnV)}{\partial L} = 0 \qquad 7.6$$

During the l-lysine monohydrochloride purification the amount of solvent (water) is kept constant and only antisolvent (ethanol) will be added into the crystallizer. Therefore, this set up is a semibatch system, and thus the working volume of the system varies with time. According to Randolph and Larson [44] and Wey [59], in this case the population balance can be expressed on the basis of the total operating volume of the crystallizer rather than the working volume. However, since l-lysine monohydrochloride is practically insoluble in ethanol, ethanol was chosen be treated as an inert that does not effect the volume in the crystallizer. Thus, only the volume of water will be considered in these calculations.

$$\tilde{n} = nV \qquad 7.7$$

Now, the population balance will be

$$\frac{\partial \tilde{n}}{\partial t} + \frac{\partial(\tilde{n}\, G)}{\partial L} = 0 \qquad 7.8$$

This equation will be solved using the definition of moments

$$m_i = \int_0^\infty \tilde{n} L^i dL \qquad 7.9$$

Multiplying by L^i and integrating over dL [59], the population balance will be expressed as

$$\frac{dm_i}{dt} + \int_0^\infty L^i \frac{\partial}{\partial L}(G\tilde{n})dL = 0 \qquad 7.10$$

and for size-independent growth the first four moments will be

$$\frac{dm_0}{dt} = \tilde{n}_0 G = B_0 \qquad 7.11$$

$$\frac{dm_1}{dt} = m_0 G \qquad 7.12$$

$$\frac{dm_2}{dt} = 2 m_1 G \qquad 7.13$$

$$\frac{dm_3}{dt} = 3 m_2 G \qquad 7.14$$

Using the definition of a derivative and the crystal suspension density, m_T, from Wey [59] and Randolph and Larson [44]

$$m_T = k_v \rho_c m_3 \qquad 7.15$$

the nucleation rate in Equation 7.11 can be iterated by estimating the nucleation rate behavior during the crystallization. Figure 7.6 shows the estimated nucleation behavior during the crystallization for various ethanol addition rates. The initial nucleation rates are of the same order of magnitude as the nucleation rates published in Mina-Mankarios and Pinder [31]. This is

the only related article to publish any kinetic data. Figure 7.7 shows the results for 1 ml/min ethanol addition rate.

7.4 Conclusions

Nucleation cell experiments demonstrated that the growth rate of l-lysine monohydrochloride is size-independent. The experiments also showed that the addition of ethanol does not have a significant effect on the growth rate. Seeded experiments were used to obtain an estimate for the overall growth rate in the crystallizer. The growth rate was further used with the population balance to iterate a prediction for the nucleation rate.

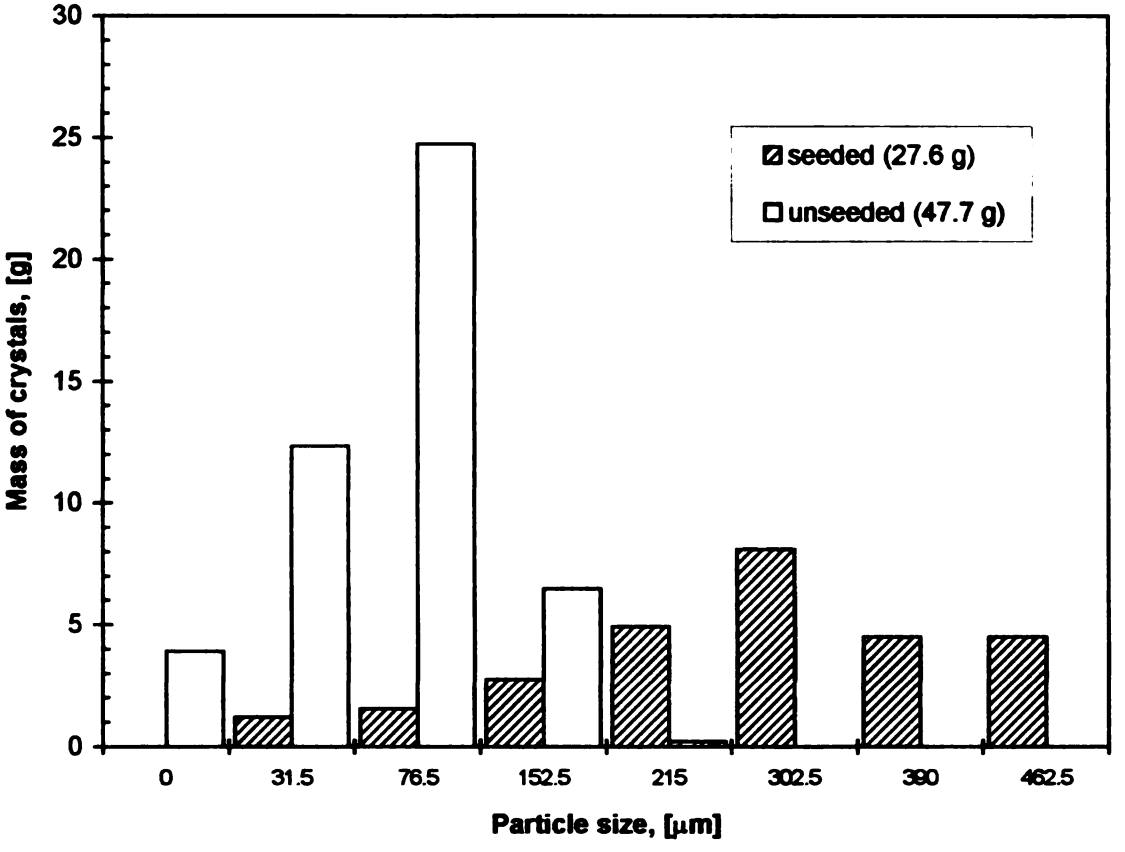

Figure 7.5. Crystal size distribution of the fines after 30 minutes of l-lysine monohydrochloride crystallization at 30 °C. Antisolvent was added at 1 ml/min and the seeds for the seeded experiments were the 500-600 µm sieve fraction.

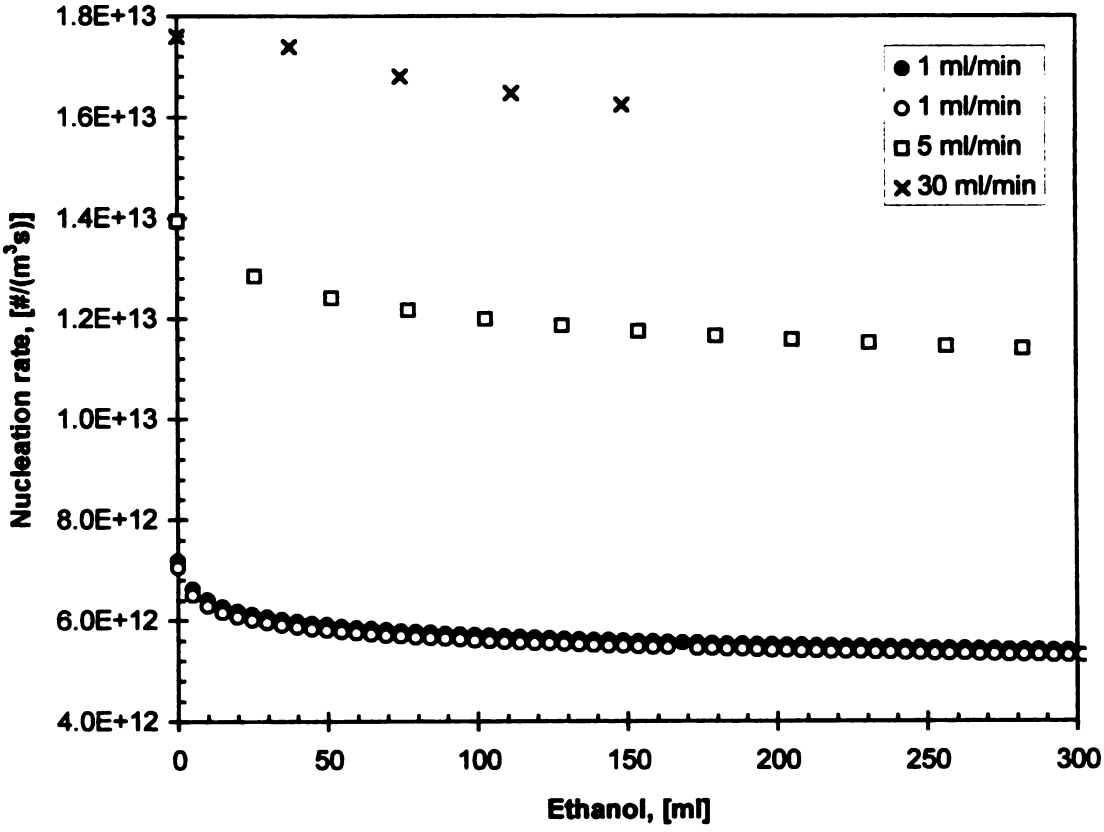

Figure 7.6. Predicted nucleation behavior during crystallization.

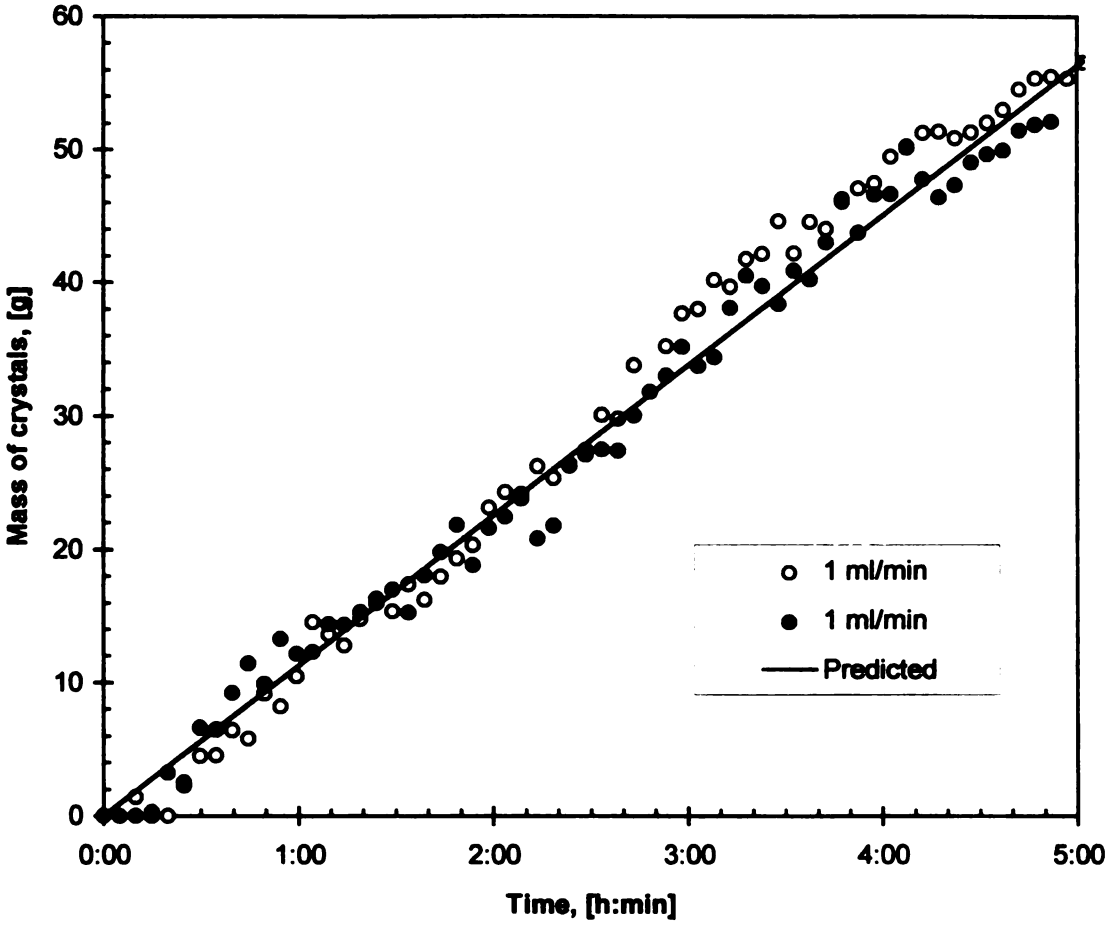

Figure 7.7. Experimental and predicted yield for unseeded experiments using the predicted nucleation and growth rates.

Chapter 8

INFLUENCE OF ETHANOL ADDITION RATE ON PARTICLE SIZE DISTRIBUTION

8.1 Introduction

There are very few studies dealing with the fundamentals of antisolvent crystallization, even though it is a commonly used method for both purification and separation in the food and pharmaceutical industries. In spite of the importance of this process, current methods for monitoring the influence of the antisolvent addition rate on the final crystal size distribution are lacking. In Uusi-Penttilä and Berglund [56] it has been shown that the dependence of the crystal size distribution on the antisolvent addition rate is significant.

In this chapter the effect of the antisolvent addition rate on the crystal mass, supersaturation, weight based average crystal size, and crystal size distribution is addressed. Attenuated total reflection Fourier transform infrared spectroscopy was used for the *in situ* monitoring of the system.

This chapter is based on the article titled "Spectroscopic monitoring of environmentally benign anti-solvent crystallization" by Uusi-Penttilä and Berglund [56] and on a manuscript titled "*In situ* monitoring of antisolvent crystallization using attenuated total reflection Fourier transform infrared spectroscopy" by Uusi-Penttilä and Berglund [55].

8.2 Crystal mass

The antisolvent addition decreases the solubility of the solute in the solvent significantly. This indicates that the yields obtained using this crystallization method should be very high. The yield increases from barely 10 % up to about 90 % as the amount of ethanol increases from 0.1 to 2 grams per gram of water. The 90 % yield is much better than yields achieved with other methods, such as cooling crystallization.

Using the calibration curves presented in Chapter 5, the composition of the liquid phase in the crystallizer can be monitored *in situ*. The mass of ethanol in the crystallizer is obtained from Equation 5.4

$$m_e = \frac{(1 - A_r)\, m_w}{A_r - 0.69} \qquad 5.4$$

and the mass of dissolved l-lysine monohydrochloride from Equation 5.7

$$m_L = \frac{D\,(m_e + m_w)}{43.4 - D} \qquad 5.7$$

Thus the l-lysine monohydrochloride mass balance can be used to determine the amount of solids in the crystallizer at any time during the crystallization.

$$m_s = m_{Lo} - m_L \qquad 8.1$$

where m_{Lo} is the initial mass of l-lysine monohydrochloride, and m_L is the mass of l-lysine monohydrochloride at time t. Figure 8.1 demonstrates the increase in the crystal mass, m_s, during crystallization experiments at different antisolvent addition rates.

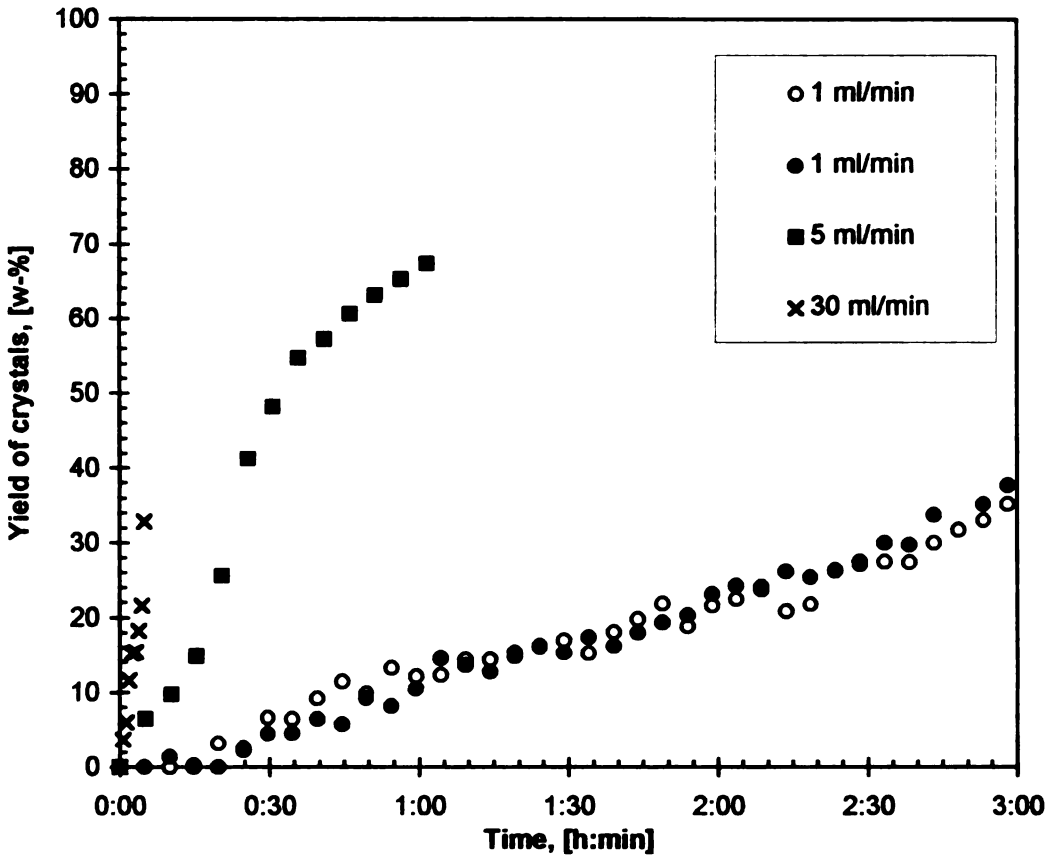

Figure 8.1. The effect of ethanol addition on the increase in crystal mass during the l-lysine monohydrochloride crystallization at 30 °C.

Since the trends for the increasing mass are linear, the following equation was obtained to predict the amount of solids in the crystallizer.

$$m_s = 0.917\, k_v\, \rho_c\, Q_e\, t \qquad 8.2$$

where k_v is the volume shape factor assuming spherical particles, ρ_c is the density of l-lysine monohydrochloride, Q_e is the antisolvent addition rate, and t is time.

8.3 Supersaturation

ATR FTIR data can be used to monitor the level of bulk supersaturation in the crystallizer. It has been suggested that the optimal operating mode for a batch crystallizer would be to use a constant level of supersaturation [34]. This is especially true for antisolvent crystallization where controlling the excessive nucleation due to the antisolvent addition is one of the biggest problems.

The relative bulk supersaturation in the crystallizer during an experiment was calculated from infrared and solubility data using the following equation

$$\sigma = \frac{c_L - c_{L,eq}}{c_{L,eq}} = \frac{m_L - m_{L,eq}}{m_{L,eq}} \qquad 8.3$$

where m_L is obtained from Equation 5.7 and $m_{L,eq}$ is solved from the solubility equation 4.1

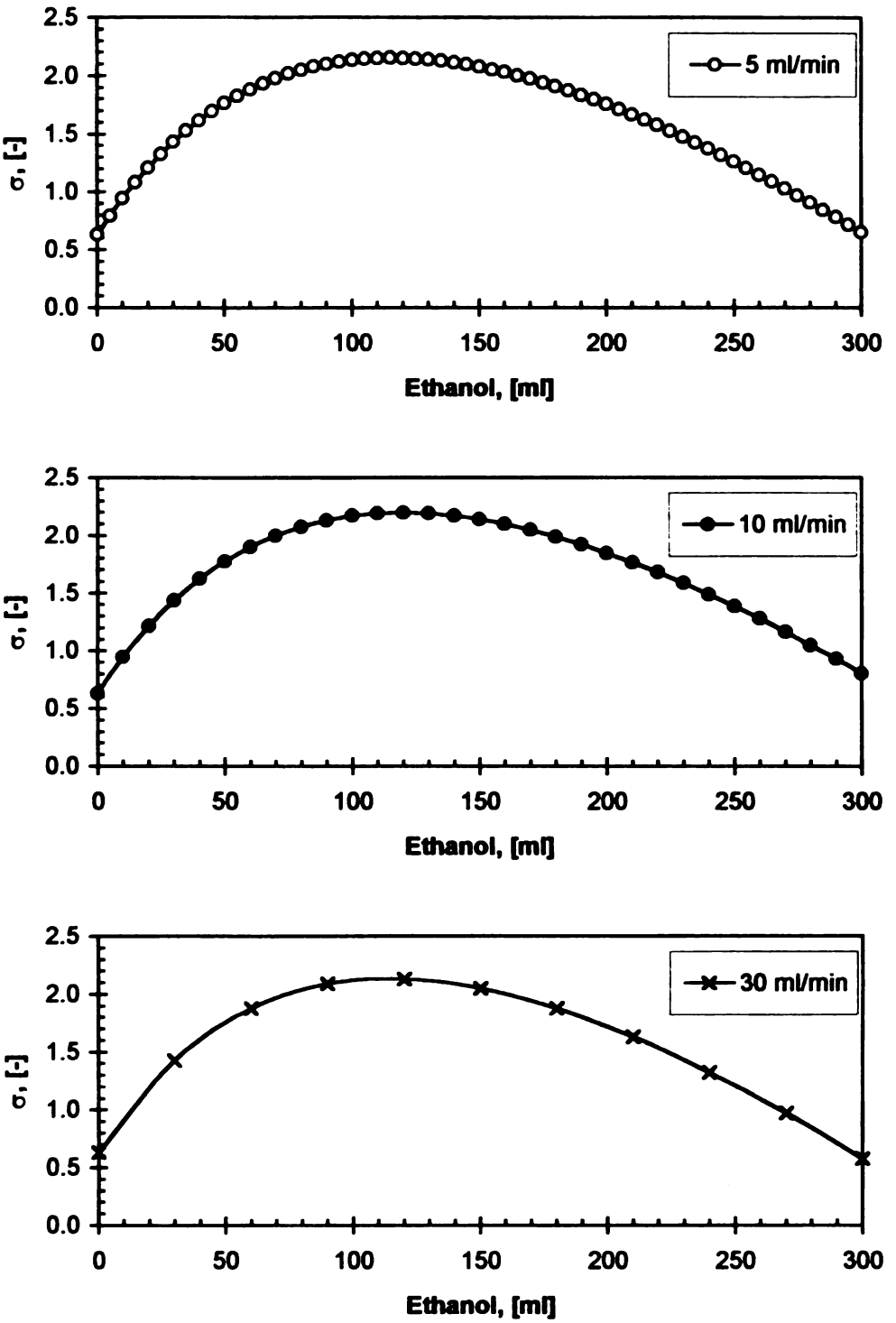

Figure 8.2. Relative bulk supersaturation for l-lysine monohydrochloride purification as a function of added ethanol for various ethanol addition rates.

$$m_{L,eq} = 0.13 \left(\frac{\rho_e Q_e t + \rho_w V_w}{0.18 + \frac{\rho_e Q_e t}{\rho_w V_w}} \right) \qquad 8.4$$

where ρ_e is the density of ethanol, Q_e is the volumetric ethanol flowrate, t is the time, ρ_w is the density of water, and V_w is the volume of water. The profiles for the relative bulk supersaturation using various ethanol addition rates are shown in Figure 8.2.

As can be seen from Figure 8.2, monitoring the bulk supersaturation exposed an interesting feature of the l-lysine monohydrochloride purification system. The effect of the ethanol addition is so strong that the bulk supersaturation depends only on the ethanol concentration and hardly on the ethanol addition rate. However, it should be kept in mind that the local supersaturation at the point of the ethanol addition can be very different from the bulk supersaturation.

8.4 Weight based mean crystal size

The weight based mean crystal size, L_{wm}, is determined from the sieved crystal size distributions using Equation 7.4.

$$L_{wm} = \Sigma(L_i w_i) / \Sigma w_i \qquad 7.4$$

In Figure 8.3 the weight based mean crystal size is plotted as a function of ethanol addition rate. The following correlation is found from the data

$$L_{wm} = 800 \exp(-0.022 Q_e) + 40 \qquad 8.5$$

where L_{wm} is the weight based mean size in mm, and Q_e is the volumetric ethanol addition rate in ml/min.

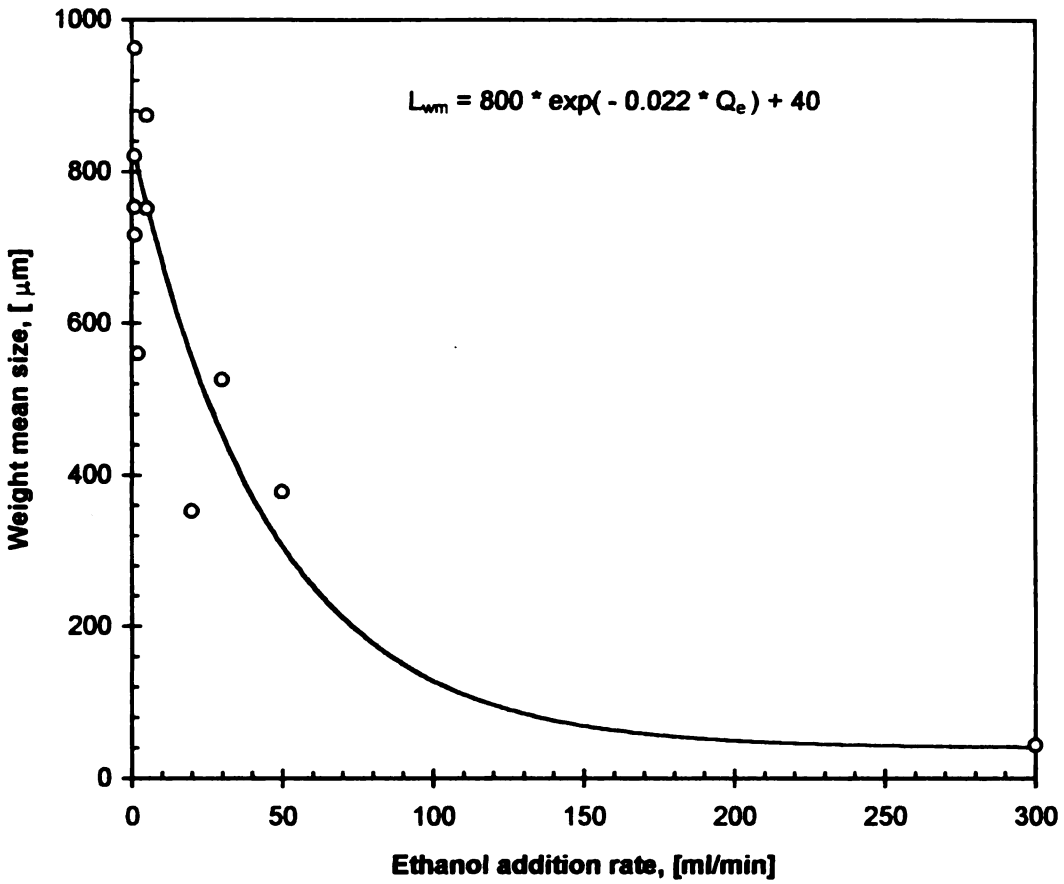

Figure 8.3. Weight mean size of crystals as a function of ethanol addition rate at 30 °C. The initial solution contained 42 w-% of l-lysine monohydrochloride in water.

8.5 Crystal size distribution

Antisolvent crystallization produces very narrow crystal size distributions. The crystal size distributions for sixteen experiments were determined by sieving and further analyzed statistically according to the procedure in Mullin [34]. Since a $2^{1/4}$ sieve series was used, an arithmetic mean was used for a mean size of each sieve cut. The standard deviation for the distribution was calculated from

$$\sigma = \frac{L_{84\%} - L_{16\%}}{2} \qquad 8.6$$

where $L_{84\%}$ is the particle size at 84% on the cumulative undersize percentage plot, and $L_{16\%}$ is the particle size at 16% on the cumulative undersize percentage plot.

The coefficient of variation was calculated from the standard deviation and weight mean size

$$CV = \frac{\sigma}{L_{wm}} \qquad 8.7$$

An average coefficient of variation for sixteen experiments was 0.526. This is remarkably close to 0.52, the coefficient of variation for a Gaussian distribution. The main argument against using the Gaussian distribution to predict particle size distributions is the symmetry of the distribution. Due to the symmetry, the distribution predicts negative particle sizes. Therefore, the experimental l-lysine monohydrochloride data was also fitted using log-normal and gamma distributions. These distributions overcome the problem of negative particle sizes. However, the best fit was obtained using the Gaussian distribution, and this distribution was used to fit the crystal size distributions for l-lysine monohydrochloride purification.

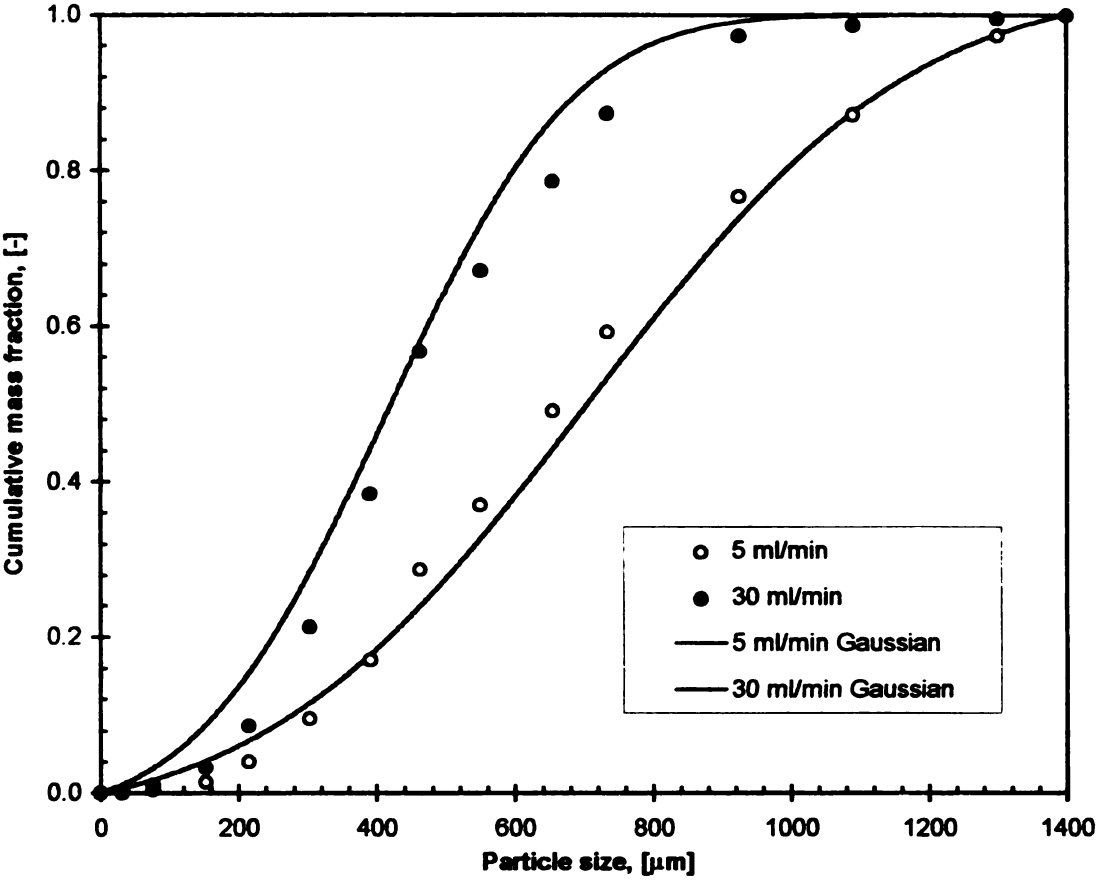

Figure 8.4. Experimental and predicted cumulative crystal size distributions for 5 ml/min and 30 ml/min antisolvent addition rates. The l-lysine monohydrochloride purification was done at 30 °C and the initial solution contained 42 w-% of l-lysine monohydrochloride in water.

Equation 8.8 gives the Gaussian distribution.

$$f(L) = \frac{1}{\sigma\sqrt{2\pi}} \exp\left[-\frac{(L - L_{wm})^2}{2\sigma^2}\right] \qquad 8.8$$

This equation is used to predict the crystal size distributions for 5 ml/min and 30 ml/min antisolvent addition rates. The weight based mean size is obtained from Equation 8.5, and the coefficient of variation is assumed to be 0.52. The results are presented in Figure 8.4. Comparison to experimental data shows that this approach predicts the cumulative particle size distributions well.

8.6 Conclusions

The effect of the antisolvent addition rate on the crystallization was investigated. It was shown that the weight based mean particle size and the crystal mass were strongly affected by the antisolvent addition rate. The bulk supersaturation was only affected by the antisolvent concentration in the crystallizer and not by the antisolvent addition rate. The shape of the crystal size distribution was Gaussian using this crystallization method, and it was not affected by varying antisolvent addition rates.

Chapter 9

CONCLUSIONS

This thesis is basic study of a batch antisolvent crystallization. Antisolvent crystallization is an excellent method for crystallization when a narrow particle size distribution and high yields are desired. It is also effective for heat sensitive materials, since the crystallization can be achieved at low temperatures. The objective was to find an operating procedure that produces a desired particle size distribution.

Since antisolvent crystallization is a three component system, the interactions between the solvent and the antisolvent were studied first. It was shown that the influence of the antisolvent addition can be much more dramatic than expected based on an ideal system. Therefore, a new method for estimating the polarity of a binary mixture was presented.

Chapter 2 introduced the method where the changes in the emission maximum of a polarity sensitive solvatochromic probe molecule were related to polarity changes of common solvents. It was also shown how to use this method to estimate dielectric constants for less known solvents.

In Chapter 3 the same approach was used to study the polarity behavior of various binary mixtures. The nonideality in the ethanol-water system was due to hydrogen bonding effects. The results indicated that a small amount of ethanol caused a significant change in the system polarity, and thus, a very sharp decrease in solubility.

No solubility data were found in the literature for l-lysine monohydrochloride in water or ethanol. Therefore, the solubility of l-lysine monohydrochloride in water, in ethanol and in mixtures of ethanol and water was determined. The l-lysine monohydrochloride solubility in water was found to be only slightly temperature dependent, and l-lysine monohydrochloride was practically insoluble in ethanol. The solubility in mixtures of ethanol and water decreased considerably with the ethanol concentration. This was exploited in the crystallization.

Attenuated total reflection Fourier transform spectroscopy was used for *in situ* monitoring of the crystallization. In Chapter 5 the calibration curves for both ethanol concentration and l-lysine monohydrochloride concentration were generated. These were then used in Chapters 7 and 8 to obtain accurate information about the crystallization.

The kinetics of the system were studied using a nucleation cell and seeded batch experiments. The nucleation cell experiments confirmed that the growth rate of l-lysine monohydrochloride is size-independent. These experiments also indicated that ethanol does not change the growth behavior significantly. The growth of seed crystals in seeded batch experiments was then used to estimate overall growth rates for l-lysine monohydrochloride crystals. Estimates for the nucleation rates were iterated using the population balance. However, since the nucleation rate is very sensitive to the operating conditions, the numerical values presented in this thesis only reflect the order of magnitude of the nucleation rate.

Chapter 7 discussed the effect of the antisolvent addition rate on the product specifications. This was studied by sieving the crystallized product. A relationship between the weight based average particle size and the antisolvent addition rate was developed. This can be used to predict the antisolvent addition rate to obtain a desired average size for the particle size distribution. The experiments confirmed that the crystal size distributions obtained in the antisolvent crystallization are narrow, and not affected by the antisolvent addition rate. Chapter 7 addressed also the effect of the antisolvent addition rate on parameters related to the operation of the crystallizer. The

ATR FTIR data was used to analyze this. A linear relationship was found between the change in the crystal mass during the crystallization and the antisolvent addition rate. The bulk supersaturation was obtained from the *in situ* measurements as well. It was shown that the bulk supersaturation was only a function of antisolvent concentration and not of antisolvent addition rate. Therefore, controlling the level of bulk supersaturation is impossible when the antisolvent is added at constant flowrate into the crystallizer.

The study of the bulk supersaturation introduced the main problem of the constant antisolvent addition rate approach. Since the level of bulk supersaturation cannot be controlled, and much less the level of local supersaturation at the point of antisolvent addition, the addition of the antisolvent causes excessive nucleation during the crystallization. This nucleation in turn produces a large number of very fine particles which leads to a less uniform crystal size and possible problems in the downstream processing. This same problem occurs also in other batch crystallization processes, like cooling and evaporative crystallizations. For cooling crystallization it has been found that the desired mode of operation is that of constant supersaturation, effectively controling the excessive nucleation and thus producing better crystals. For antisolvent crystallization there are two different possibilities to control the level of bulk supersaturation: seeding and adding solvent into the crystallizer along with the antisolvent. As was shown in Chapter 6, seeding effectively reduces the amount of nuclei in the crystallizer. Also, the quality of the grown seed crystals is very good. The other approach of also adding solvent into the crystallizer will decrease the amount of nucleation, but it also decreases the yields. Both of these approaches would need more experimental work to be exploited further.

As a result of this research, the antisolvent approach is already used in industry for small scale l-lysine monohydrochloride purification. The process has been successfully scaled-up to five times the original laboratory scale. Compared to the previously used cooling crystallization this method produces significantly higher yields and better quality crystals. Also, since the crystal size distribution is very narrow, the milling step is no longer needed.

APPENDIX

APPENDIX

Table A.1. Data for Figure 2.1. The Nile Red absorption and emission maxima in various esters and alcohols. The emission spectra were excited at absorption maxima.

SOLVENT	ABSORPTION [nm]	EMISSION [nm]
methanol	557	640
ethanol	549	635
n-propanol	546	633
n-butanol	547	631
n-pentanol	546	632
n-hexanol	544	629
n-octanol	541	626
ethyl formate	526	615
propyl formate	526	611
ethyl acetate	521	596
ethyl acetoacetate	535	614
butyl acetate	521	584
methyl propionate	521	588
methyl butyrate	520	586
ethyl butyrate	519	584
ethyl lactate	547	636
dimethyl succinate	533	606
dimethyl maleate	538	621
dimethyl glutarate	525	605
dimethyl adipate	530	602
diethyl succinate	531	599
diethyl maleate	534	607
diethyl fumarate	532	598
diethyl l-tartrate	550	640
dibutyl fumarate	528	607
dibutyl l-tartrate	545	633
dibutyl itaconate	528	598
dibutyl maleate	530	611
triethyl citrate	535	619

APPENDIX

Table A.2. Data for Figure 4.1. Solubility of l-lysine monohydrochloride in water as a function of temperature.

Temperature [°C]	L-lysine monohydrochloride concentration [w-%]
20.0	39.4
25.0	41.3
25.0	40.1
25.8	40.1
27.0	42.1
27.3	42.4
27.7	42.4
29.0	43.0
30.5	43.8
30.8	44.4
30.9	42.4
31.0	44. 6
33.0	45.3
33.6	45.1
35.1	44.6
44.9	50.2
45.2	50.3

APPENDIX

Table A.3. Data for Figure 4.2. Solubility of l-lysine monohydrochloride in various binary mixtures of water and ethanol at 30 ± 1 °C.

mass of ethanol / mass of water [$g_{ethanol}$ /g_{water}]	l-lysine monohydrochloride in solution [g_{llmhc} /g_{water}]
0.00	0.73
0.22	0.42
0.27	0.45
0.26	0.35
0.61	0.22
0.29	0.35
0.42	0.29
0.42	0.29
1.62	0.08
0.75	0.17
0.91	0.10
0.75	0.15
0.90	0.11
0.84	0.11
0.90	0.10
0.90	0.12
0.53	0.18
1.58	0.04
2.63	0.02
2.63	0.01
6.83	0.00
4.73	0.01
0.11	0.48
0.21	0.36
1.05	0.07
2.68	0.02
1.77	0.05
2.17	0.03

APPENDIX

Table A.4. Data for Figure 5.2. The penetration depth of the evanescent wave for pure water and pure ethanol as a function of wavenumber. The data were calculated using Equation 5.4.

wavenumber [cm^{-1}]	penetration depth in water [μm]	penetration depth in ethanol [μm]
700	3.406	3.482
800	2.981	3.047
900	2.649	2.709
1000	2.384	2.438
1100	2.168	2.216
1200	1.987	2.031
1300	1.834	1.875
1400	1.703	1.741
1500	1.590	1.625
1600	1.490	1.524
1700	1.403	1.434
1800	1.325	1.354
1900	1.255	1.283
2000	1.192	1.219
2100	1.135	1.161
2200	1.084	1.108
2300	1.037	1.060
2400	0.994	1.016
2500	0.954	0.975
2600	0.917	0.938
2700	0.883	0.903
2800	0.852	0.871
2900	0.822	0.841
3000	0.795	0.813
3100	0.769	0.786
3200	0.745	0.762
3300	0.723	0.739
3400	0.701	0.717
3500	0.681	0.696
3600	0.662	0.677
3700	0.644	0.659
3800	0.627	0.641
3900	0.611	0.625
4000	0.596	0.609

APPENDIX

Table A.5. Data for Figure 5.5. Relative absorbance as a function of ethanol weight percentage.

w-% of ethanol	LOG(A_{1042} / A_{1110})	llmhc	w-% of ethanol	LOG(A_{1042} / A_{1110})	llmhc
0.0	1.003891	yes	34.6	0.851830	yes
0.0	1.002844	yes	35.9	0.844773	yes
0.0	1.003247	yes	36.1	0.827419	yes
0.0	1.003134	yes	37.0	0.862060	no
0.0	0.996155	no	37.0	0.856584	no
0.0	1.006393	no	37.4	0.839116	yes
0.0	0.997069	no	38.5	0.818246	yes
0.0	1.007596	yes	38.5	0.814135	yes
0.0	1.003628	yes	40.2	0.829758	yes
1.7	0.989849	yes	40.8	0.809942	yes
5.9	0.970487	yes	40.8	0.838364	yes
6.9	0.966018	yes	41.3	0.813880	yes
9.2	0.956335	yes	42.7	0.822030	yes
11.1	0.940956	yes	42.7	0.818690	yes
13.0	0.938648	yes	42.9	0.802030	yes
13.5	0.929001	yes	43.6	0.817957	yes
15.0	0.960044	yes	43.9	0.795135	yes
15.6	0.928817	yes	44.0	0.838722	no
15.7	0.925468	yes	44.0	0.834154	no
15.8	0.916796	yes	44.9	0.795578	yes
16.4	0.937143	no	46.1	0.810716	yes
16.4	0.931872	no	46.7	0.790222	yes
18.3	0.915245	yes	46.8	0.783865	yes
20.0	0.898118	yes	48.3	0.798029	yes
23.0	0.895276	yes	48.3	0.801989	yes
23.9	0.881606	yes	48.4	0.779543	yes
23.9	0.880869	yes	48.4	0.778475	yes
26.1	0.903208	yes	49.5	0.820253	no
26.1	0.887121	yes	50.5	0.813970	no
27.2	0.876260	yes	50.6	0.795974	yes
27.2	0.877580	yes	52.8	0.785550	yes
27.3	0.864954	yes	52.8	0.783068	yes
28.2	0.892743	no	52.8	0.789995	yes
28.2	0.887394	no	52.8	0.785631	yes
30.5	0.849937	yes	54.1	0.806806	no
30.9	0.861286	yes	54.1	0.802808	no
32.0	0.842387	yes	100.0	0.706624	no
33.4	0.837980	yes	100.0	0.706218	no
34.2	0.859437	yes	100.0	0.706696	no
34.3	0.849958	yes	100.0	0.706339	no

APPENDIX

Table A.6. Data without ethanol for Figure 5.6. Difference of the second derivative peaks at 1411 cm^{-1} and 1432 cm^{-1} as a function of the weight fraction of l-lysine monohydrochloride.

w-% of llmhc	*D*
20.1	7.5455
26.0	10.8680
29.4	13.4487
33.4	15.1594
35.6	16.2807
0.0	0.0885
5.0	2.6185
10.0	4.4791
15.0	5.8755

APPENDIX

Table A.7. Data with ethanol for Figure 5.6. Difference of the second derivative peaks at 1411 cm^{-1} and 1432 cm^{-1} as a function of the weight fraction of l-lysine monohydrochloride.

w-% of llmhc	*D*	w-% of llmhc	*D*
0.0	1.2978	19.8	8.6312
0.0	1.5019	20.9	9.2622
0.0	0.7365	20.9	8.7713
0.0	0.8436	21.2	9.2780
0.0	1.5876	22.1	9.9542
0.0	1.9218	23.4	10.3646
0.0	1.8485	24.2	10.5069
0.0	2.0384	24.2	9.9752
0.0	2.1293	24.9	10.9160
0.0	0.5892	26.0	11.1057
0.0	0.7167	26.7	11.4068
0.0	0.9904	28.2	12.1259
0.0	1.1170	28.7	13.4064
0.0	1.3452	28.7	11.9348
0.0	1.3440	28.7	12.5894
0.0	1.3796	29.7	14.5051
0.0	0.8691	32.1	13.7347
0.0	1.0637	33.8	14.5476
16.4	6.2071	34.1	16.7578
17.0	7.5141	34.7	14.3204
17.1	7.9027	35.6	14.9418
17.9	8.1602	37.7	15.8416
18.4	7.1804	40.1	17.0472
18.4	7.1439	40.1	16.5054
18.8	8.3451	40.1	17.0968
18.9	8.3531		

APPENDIX

Table A.8. Data without Ethanol for Figure 7.2. Spherical equivalent diameter for single crystals in a seeded nucleation cell.

Time [h:min]	Spherical equivalent diameter [mm]	Time [h:min]	Spherical equivalent diameter [mm]
0:00	0.529	0:15	0.857
0:00	0.357	0:20	0.668
0:00	0.265	0:20	1.074
0:00	0.219	0:20	1.066
0:00	0.403	0:20	1.007
0:00	0.263	0:20	1.074
0:00	0.224	0:20	0.668
0:00	0.155	0:30	0.748
0:07	0.772	0:30	0.814
0:07	0.656	0:30	1.267
0:07	0.610	0:30	1.253
0:07	0.508	0:30	1.215
0:10	0.529	0:40	1.391
0:10	0.535	0:40	1.456
0:10	0.852	0:45	1.336
0:10	0.553	0:55	1.674
0:10	0.658	1:00	1.858
0:10	0.575	1:11	2.438
0:15	0.994	1:20	2.679
0:15	0.990	1:31	3.018
0:15	0.818	1:42	3.103

APPENDIX

Table A.9. Data with Ethanol for Figure 7.2. Spherical equivalent diameter for single crystals in a seeded nucleation cell.

Time [h:min]	Spherical equivalent diameter [mm]	Time [h:min]	Spherical equivalent diameter [mm]
0:00	0.239	0:25	1.128
0:00	0.359	0:25	0.888
0:00	0.350	0:25	1.175
0:00	0.359	0:30	0.930
0:05	0.409	0:30	1.278
0:05	0.522	0:30	1.056
0:05	0.479	0:30	1.276
0:05	0.535	0:34	0.944
0:10	0.535	0:34	1.356
0:10	0.659	0:39	1.043
0:10	0.628	0:39	1.497
0:10	0.705	0:39	1.206
0:10	0.667	0:39	1.438
0:10	0.757	0:42	1.014
0:15	0.648	0:42	1.495
0:15	0.814	0:42	1.664
0:15	0.728	0:42	1.576
0:15	0.867	0:42	1.391
0:19	0.829	0:52	1.894
0:19	0.997	0:52	1.755
0:20	0.731	0:52	1.525
0:20	0.977	1:02	2.073
0:20	0.857	1:02	1.924
0:20	1.016	1:02	1.672
0:25	0.818	1:12	2.212
0:25	1.116	1:12	2.054
0:25	0.947	1:12	1.756

APPENDIX

Table A.10. Data for Figure 7.3. Mass of l-lysine monohydrochloride crystals retained on the sieves after 2, 5, and 10 minutes of crystallization. The experiment was done at 30 °C and the ethanol addition rate was 20 ml/min. The average seed size was 550 μm and the mass of seeds was 10 g.

Particle size, [μm]	Mass, [g]		
	2 min	5 min	10 min
31.5	0.46	0.18	0.36
76.5	0.64	0.65	1.16
152.5	0.99	2.62	3.51
215.5	1.04	8.79	8.61
302.5	1.15	13.58	13.01
390.0	0.90	8.32	12.22
462.5	1.11	3.57	5.53
550.0	2.75	3.96	3.91
655.0	6.29	3.84	4.23
735.0	6.72	17.01	17.65
925.0	0.98	7.69	17.67
1090.0	0.96	5.29	15.55
1300.0	0.96	5.29	2.08

APPENDIX

Table A.11. Data for Figure 7.4. Estimate for the overall growth rate as a function of ethanol addition rate from seeded experiments.

Time [min]	Weight based mean particle size [μm]		
	1 ml/min	5 ml/min	20 ml/min
0	463	550	550
2			708
5			796
10			884
15	634	844	
30	804	931	
45		1028	
60	896		
growth rate	7.1	10	31

APPENDIX

Table A.12. Data for Figure 7.5. Crystal size distribution of the fines after 30 minutes of crystallization. Antisolvent was added at 1 ml/min and the seeds for the seeded experiments were the 500-600 μm sieve fraction.

Average size [μm]	Seeded [g]	Unseeded [g]
0.0	0.00	3.93
31.5	1.22	12.34
76.5	1.56	24.72
152.5	2.75	6.48
215.0	4.92	0.20
302.5	8.11	0.00
390.0	4.49	0.00
462.5	4.51	0.00
	27.6	47.7

APPENDIX

Table A.13. Data for Figure 7.6. Predicted nucleation behavior during crystallization.

Ethanol	Nucleation rate		Ethanol	Nucleation rate	
[ml]	1 ml/min	1 ml/min	[ml]	1 ml/min	1 ml/min
0.00	7.18E+12	7.05E+12	153.45	5.58E+12	5.48E+12
4.95	6.63E+12	6.50E+12	158.40	5.57E+12	5.47E+12
9.90	6.40E+12	6.28E+12	163.35	5.57E+12	5.46E+12
14.85	6.28E+12	6.16E+12	168.30	5.56E+12	
19.80	6.19E+12	6.07E+12	173.25	5.55E+12	5.44E+12
24.75	6.12E+12	6.00E+12	178.20	5.54E+12	5.44E+12
29.70	6.06E+12	5.95E+12	183.15	5.53E+12	5.43E+12
34.65	6.01E+12	5.90E+12	188.10	5.53E+12	5.42E+12
39.60	5.97E+12	5.86E+12	193.05	5.52E+12	5.42E+12
44.55	5.94E+12	5.83E+12	198.00	5.51E+12	5.41E+12
49.50	5.91E+12	5.80E+12	202.95	5.51E+12	5.40E+12
54.45	5.88E+12	5.77E+12	207.90	5.50E+12	5.40E+12
59.40	5.85E+12	5.74E+12	212.85	5.49E+12	5.39E+12
64.35	5.83E+12	5.72E+12	217.80	5.49E+12	5.38E+12
69.30	5.81E+12	5.70E+12	222.75	5.48E+12	5.38E+12
74.25	5.79E+12	5.68E+12	227.70	5.47E+12	5.37E+12
79.20	5.77E+12	5.66E+12	232.65	5.47E+12	5.36E+12
84.15	5.75E+12	5.64E+12	237.60	5.46E+12	5.36E+12
89.10	5.74E+12	5.63E+12	242.55	5.46E+12	5.35E+12
94.05	5.72E+12	5.61E+12	247.50	5.45E+12	5.35E+12
99.00	5.71E+12	5.60E+12	252.45	5.45E+12	5.34E+12
103.95	5.69E+12	5.59E+12	257.40	5.44E+12	5.34E+12
108.90	5.68E+12	5.57E+12	262.35	5.44E+12	5.33E+12
113.85	5.67E+12	5.56E+12	267.30	5.43E+12	5.33E+12
118.80	5.66E+12	5.55E+12	272.25	5.43E+12	5.32E+12
123.75	5.64E+12	5.54E+12	277.20	5.42E+12	5.32E+12
128.70	5.63E+12	5.53E+12	282.15	5.42E+12	5.31E+12
133.65	5.62E+12	5.52E+12	287.10	5.41E+12	5.31E+12
138.60	5.61E+12	5.51E+12	292.05	5.41E+12	5.30E+12
143.55	5.60E+12	5.50E+12	297.00	5.40E+12	5.30E+12
148.50	5.59E+12	5.49E+12	301.95		5.30E+12

APPENDIX

Table A.14. Data for Figure 7.6. Predicted nucleation behavior during crystallization.

Ethanol [ml]	Nucleation rate 5 ml/min	Ethanol [ml]	Nucleation rate 30 ml/min
0.00	1.39E+13	0.00	1.76E+13
25.75	1.28E+13	19.00	1.80E+13
51.42	1.24E+13	37.50	1.74E+13
77.08	1.22E+13	56.00	1.70E+13
102.75	1.20E+13	74.50	1.68E+13
128.33	1.18E+13	93.00	1.66E+13
153.92	1.17E+13	111.50	1.65E+13
179.58	1.17E+13	130.00	1.63E+13
205.25	1.16E+13	148.50	1.62E+13
230.92	1.15E+13		
256.58	1.14E+13		
282.25	1.14E+13		
307.92	1.13E+13		

APPENDIX

Table A.15. Data for Figure 7.7. Experimental and predicted yield for unseeded experiments using the predicted nucleation and growth rates.

Time [h:min:s]	Yield (x) [w-%]	Yield (o) [w-%]	Predicted [w-%]	Time [h:min:s]	Yield (x) [w-%]	Yield (o) [w-%]	Predicted [w-%]
00:00:00	0.0	0.0	0.0	02:33:27	27.5	30.1	29.3
00:04:57	0.0	0.0	1.1	02:38:24	27.4	29.8	30.2
00:09:54	0.0	1.4	2.1	02:43:21	30.0	33.8	31.1
00:14:51	0.0	0.3	3.1	02:48:18	31.8	35.2	32.0
00:19:48	3.2	0.0	4.1	02:53:15	33.0	37.7	32.9
00:24:45	2.5	2.3	5.1	02:58:12	35.2	38.0	33.8
00:29:42	6.6	4.5	6.1	03:03:09	33.7	38.0	34.7
00:34:39	6.5	4.5	7.1	03:08:06	34.4	40.2	35.6
00:39:36	9.2	6.4	8.0	03:13:03	38.1	39.7	36.5
00:44:33	11.5	5.8	9.0	03:18:00	40.6	41.8	37.4
00:49:30	9.9	9.2	9.9	03:22:57	39.8	42.2	38.3
00:54:27	13.3	8.2	10.9	03:27:54	38.4	44.7	39.1
00:59:24	12.2	10.5	11.8	03:32:51	41.0	42.2	40.0
01:04:21	12.3	14.5	12.8	03:37:48	40.2	44.6	40.9
01:09:18	14.4	13.6	13.7	03:42:45	43.0	44.0	41.8
01:14:15	14.4	12.8	14.7	03:47:42	46.3	46.1	42.7
01:19:12	15.3	14.8	15.6	03:52:39	43.8	47.1	43.6
01:24:09	16.3	16.0	16.5	03:57:36	46.6	47.5	44.5
01:29:06	17.0	15.3	17.4	04:02:33	46.7	49.5	45.3
01:34:03	15.3	17.4	18.4	04:07:30	50.2	50.3	46.2
01:39:00	18.1	16.2	19.3	04:12:27	47.8	51.3	47.1
01:43:57	19.8	18.0	20.2	04:17:24	46.4	51.4	48.0
01:48:54	21.8	19.3	21.1	04:22:21	47.3	50.9	48.9
01:53:51	18.8	20.3	22.0	04:27:18	49.0	51.3	49.7
01:58:48	21.6	23.1	23.0	04:32:15	49.7	52.0	50.6
02:03:45	22.5	24.3	23.9	04:37:12	50.0	53.0	51.5
02:08:42	24.1	23.8	24.8	04:42:09	51.5	54.6	52.4
02:13:39	20.8	26.2	25.7	04:47:06	51.9	55.4	53.2
02:18:36	21.8	25.4	26.6	04:52:03	52.1	55.5	54.1
02:23:33	26.4	26.2	27.5	04:57:00	49.6	55.3	55.0
02:28:30	27.1	27.4	28.4	05:01:57	55.9	56.5	55.9

APPENDIX

Table A.16. Data for Figure 8.1. The effect of ethanol addition on the increase in crystal mass during the crystallization

Time [h:min:s]	Yield, [w-%] 1 ml/min	Yield, [w-%] 1 ml/min	Time [h:min:s]	Yield, [w-%] 5 ml/min	Time [h:min:s]	Yield, [w-%] 30 ml/min
00:00:00	0.0	0.0	00:00:00	0.0	00:00:00	0.0
00:04:57	0.0	0.0	00:05:09	6.4	00:00:38	3.7
00:09:54	0.0	1.4	00:10:17	9.7	00:01:15	6.0
00:14:51	0.0	0.3	00:15:25	14.8	00:01:52	11.6
00:19:48	3.2	0.0	00:20:33	25.5	00:02:29	15.2
00:24:45	2.5	2.3	00:25:40	41.2	00:03:06	15.4
00:29:42	6.6	4.5	00:30:47	48.2	00:03:43	18.2
00:34:39	6.5	4.5	00:35:55	54.8	00:04:20	21.6
00:39:36	9.2	6.4	00:41:03	57.3	00:04:57	32.8
00:44:33	11.5	5.8	00:46:11	60.6	00:05:34	55.4
00:49:30	9.9	9.2	00:51:19	63.1		
00:54:27	13.3	8.2	00:56:27	65.3		
00:59:24	12.2	10.5	01:01:35	67.4		
01:04:21	12.3	14.5	01:06:43	69.0		
01:09:18	14.4	13.6	01:11:51	71.1		
01:14:15	14.4	12.8	01:16:59	72.5		
01:19:12	15.3	14.8	01:22:07	73.1		
01:24:09	16.3	16.0	01:27:15	72.5		
01:29:06	17.0	15.3	01:32:23	72.3		
01:34:03	15.3	17.4	01:37:31	72.4		
01:39:00	18.1	16.2	01:42:39	71.2		
01:43:57	19.8	18.0	01:47:47	71.5		
01:48:54	21.8	19.3	01:52:55	72.4		
01:53:51	18.8	20.3	01:58:03	71.1		
01:58:48	21.6	23.1	02:03:11	71.2		
02:03:45	22.5	24.3	02:08:18	71.9		
02:08:42	24.1	23.8	02:13:25	71.3		
02:13:39	20.8	26.2	02:18:33	71.8		
02:18:36	21.8	25.4	02:23:41	70.0		
02:23:33	26.4	26.2	02:28:49	68.9		
02:28:30	27.1	27.4	02:33:57	70.1		
02:33:27	27.5	30.1	02:39:04	68.0		
02:38:24	27.4	29.8	02:44:12	69.5		
02:43:21	30.0	33.8	02:49:20	69.0		
02:48:18	31.8	35.2	02:54:28	68.3		
02:53:15	33.0	37.7	02:59:35	70.1		
02:58:12	35.2	38.0				

APPENDIX

Table A.17. Data for Figure 8.2. Relative bulk supersaturation as a function of added ethanol for various ethanol addition rates.

Ethanol	Supersaturation			
[ml]	1 ml/min	5 ml/min	10 ml/min	30 ml/min
0	0.631	0.631	0.631	0.631
10	0.957	0.946	0.947	
20	1.236	1.210	1.214	
30	1.475	1.431	1.438	1.428
40	1.678	1.614	1.624	
50	1.851	1.764	1.777	
60	1.997	1.885	1.902	1.877
70	2.118	1.980	2.001	
80	2.219	2.051	2.077	
90	2.300	2.102	2.132	2.088
100	2.364	2.135	2.170	
110	2.413	2.151	2.191	
120	2.447	2.152	2.197	2.131
130	2.469	2.140	2.190	
140	2.480	2.115	2.170	
150	2.480	2.079	2.140	2.050
160	2.471	2.032	2.099	
170	2.453	1.976	2.049	
180	2.426	1.912	1.990	1.875
190	2.393	1.839	1.923	
200	2.352	1.759	1.849	
210	2.305	1.672	1.768	1.627
220	2.253	1.579	1.681	
230	2.194	1.480	1.588	
240	2.131	1.375	1.490	1.322
250	2.063	1.266	1.387	
260	1.990	1.151	1.279	
270	1.914	1.032	1.166	0.969
280	1.833	0.909	1.049	
290	1.749	0.782	0.929	
300	1.661	0.651	0.805	0.579

APPENDIX

Table A.18. Data for Figure 8.3. Weight mean size of crystals as a function of ethanol addition rate at 30 °C. The initial solution contained 42 w-% of l-lysine monohydrochloride in water.

Ethanol addition rate [ml/min]	Weight based mean size [μm]
1	962
1	821
1	754
1	717
2	560
5	874
5	752
20	352
30	526
50	378
300	44

APPENDIX

Table A.19. Data for Figure 8.4. Experimental and predicted cumulative crystal size distributions for 5 ml/min and 30 ml/min antisolvent addition rates.

Average size [μm]	Cumulative weight fraction on sieve	
	5 ml/min	30 ml/min
0.0	0.000	0.000
31.5	0.000	0.000
76.5	0.004	0.011
152.5	0.014	0.032
215.0	0.040	0.086
302.5	0.095	0.213
390.0	0.171	0.385
462.5	0.287	0.567
550.0	0.37	0.671
655.0	0.491	0.786
735.0	0.592	0.873
925.0	0.767	0.973
1090.0	0.871	0.986
1300.0	0.973	0.995
1400.0	0.999	0.999

LIST OF REFERENCES

LIST OF REFERENCES

[1]. Axiom Analytical, *Operator's Manual, DPR-200 Series Deep Immersion Probes*, Revision D, California, **1992**.

[2]. Bátor, E., Continuous crystallization of magnesium asparaginate by salting out, *Hungarian Journal of Industrial Chemistry Veszprem*, **15** (1987), 141-148.

[3]. Budavari, S., (Ed.), *The Merck Index*, 11th Ed., Merck and Co., New Jersey, **1989**.

[4]. Budz, J., Karpinski, P.H., Mydlarz, J., and Nývlt, J., Salting-out precipitation of cocarboxylase hydrochloride from aqueous solution by addition of acetone, *Ind. Eng. Chem. Prod. Res. Dev.*, **25** (1986), 657-664.

[5]. Cahill, J.E., Derivative spectroscopy: understanding its application, *American laboratory*, **11** (1979), No. 11, 79-85.

[6]. Cahill, J.E., and Padera, F.G., Derivative analysis of uv/visible spectra, *American Laboratory*, **12** (1980), No. 4, 101-112.

[7]. Coates, J.P., The industrial applications of infrared internal reflection spectroscopy, In *Internal reflection spectroscopy: theory and applications*, Mirabella, F.M., Jr., (Ed.), Marcel Dekker, New York, **1993**.

[8]. Coetzee, J.F., and Ritchie, C.D. (Ed.), *Solute-Solvent Interactions*, Vol. 2, Marcel Dekker, New York, **1976**.

[9]. Colthup, N.B., Daly, L.H., and Wiberley, S.E., *Introduction to Infrared and Raman Spectroscopy*, 3rd Ed., Academic Press, Boston, **1990**.

[10]. Davey, R.J., The role of the solvent in crystal growth from solution, *J. Cryst. Growth*, **76** (1986), 637-644.

[11]. Deye, J.F., and Berger, T.A., Nile red as a solvatochromic dye for measuring solvent strength in normal liquids and mixtures of normal liquids with supercritical and near critical fluids, *Anal. Chem.*, **62** (1990), 615-622.

[12]. Dunuwila, D.D., An investigation of the feasibility of using *in situ* ATR FTIR spectroscopy in the measurement of crystallization phenomena for research and development of batch crystallization processes, Ph.D. Dissertation, Michigan State University, **1996**.

[13]. Dunuwila, D.D., Carroll II, L.B., and Berglund, K.A., An investigation of the applicability of attenuated total reflection infrared spectroscopy for measurement of solubility and supersaturation of aqueous citric acid solutions, *J. Cryst. Growth*, **137** (1994), 561-568.

[14]. Dutta, A.K., Kamada, K., and Ohta, K., Spectroscopic studies of nile red in organic solvents and polymers, *J. of Photochem. and Photobiology, A: Chemistry*, **93** (1996), 57-64.

[15]. Gabas, N., and Laguérie, C., Batch crystallization of d-xylose by programmed cooling or by programmed adding of ethanol, *Chem. Eng. Sci.*, **47** (1992), No. 12, 3148-3152.

[16]. Ghoneim, N., and Suppan, P., Solvatochromic shifts of non-dipolar molecules in polar solvents, *Spectrochimica Acta*, **51A** (1995), No. 6, 1043-1050.

[17]. Greenspan, P., and Fowler, S.D., Spectrofluorometric studies of the lipid probe, nile red, *J. of Lipid Res.*, **26** (1985), 781-789.

[18]. Hawkes, S., Maddams, W.F., Mead, W.L., and Southon, M.J., The measurement of derivative i.r. spectra - II. Experimental measurements, *Spectrochimica Acta*, **38A** (1982), No. 4, 445-457.

[19]. Ingle, J.D., Jr., and Crouch, S.R., *Spectrochemical analysis*, Prentice-Hall, New Jersey, **1988**.

[20]. Irani, R.R., and Callis, C.F., *Particle size: measurement, interpretation, and application*, John Wiley, New York, **1963**.

[21]. Jones, A.G., Budz, J., and Mullin, J.W., Batch crystallization and solid-liquid separation of potassium sulphate, *Chem. Eng. Sci.*, **29** (1974), 1075-1087.

[22]. Jones, A.G., and Teodossiev, N.M., Microcomputer programming of dosage rate during batch precipitation, *Cryst. Res. Technol.*, **23** (1988), No. 8, 957-966.

[23]. Karpinski, P.H., and Nývlt, J., Metastable zone width in salting-out crystallization, *J. Cryst. Res. Technol.*, **18** (1983), No. 7, 959-965.

[24]. Kirk-Othmer, *Encyclopedia of Chemical Technology*, 4th Ed., John Wiley, New York, **1992**.

[25]. Kirwan, D.J., and Orella, C.J., Crystallization of biological molecules, In *Handbook of Industrial Crystallization*, Myerson, A.S. (Ed.), Butterworth-Heinemann, Maryland, **1993**.

[26] Lide, D.R., (Ed.),; *CRC Handbook of Chemistry and Physics*, 73rd Ed., CRC Press, Florida, **1992**, 9-52.

[27]. Maddams, W.F., and Mead, W.L., The measurement of derivative i.r. spectra - I. Background studies, *Spectrochimica Acta*, **38A** (1982), No. 4, 437-444.

[28]. Maddams, W.F., and Southon, M.J., The measurement of derivative i.r. spectra - III. The effect of band width and band shape on resolution enhancement by derivative spectroscopy, *Spectrochimica Acta*, **38A** (1982), No. 4, 459-466.

[29]. *Manual on testing sieving methods*, ASTM 447B, ASTM, **1985**.

[30]. Midwinter, J., and Suppan, P., Spectral shifts in solvent mixtures, *Spectrochim. Acta*, **25A** (1969), 953-958.

[31]. Mina-Mankarios, G., and Pinder, K.L., Salting out crystallization of sodium sulfate, *Can. J. Chem. Eng.*, **69** (1991), 308-324.

[32]. Mirabella, F.M., Jr., Principles, theory, and practice of internal reflection spectroscopy, In *Internal reflection spectroscopy: theory and applications*, Mirabella, F.M., Jr., (Ed.), Marcel Dekker, New York, **1993**.

[33]. Müller, G.J., and Abraham-Fuchs, K., Matrix dependence in single and multilayer IRS spectra, In *Internal reflection spectroscopy: theory and applications*, Mirabella, F.M., Jr., (Ed.), Marcel Dekker, New York, **1993**.

[34]. Mullin, J.W., *Crystallization*, 3rd Ed., Butterworth-Heinemann, Great Britain, **1993**.

[35]. Mullin, J.W., Teodossiev, N., and Söhnel, O., Potassium sulphate precipitation from aqueous solution by salting-out with acetone, *Chem. Eng. Process.*, **26** (1989), 93-99.

[36]. Myerson, A.S., Solutions and solution properties, In *Handbook of Industrial Crystallization*, Myerson, A.S. (Ed.), Butterworth-Heinemann, Maryland, **1993**.

[37]. Myerson, A.S., Decker, S.E., and Welping, F., Solvent selection and batch crystallization, *Ind. Eng. Chem. Process Des. Dev.*, **25** (1986), 925-929.

[38]. Myerson, A.S., and Ginde, R., Crystals, crystal growth, and nucleation, In *Handbook of Industrial Crystallization*, Myerson, A.S. (Ed.), Butterworth-Heinemann, Maryland, **1993**.

[39]. Nitsche, K.S., and Suppan, P., Solvatochromic shifts and polarity of solvent mixtures, *Chimia*, **36** (1982), No. 9, 346-348.

[40]. Nývlt, J., Batch salting-out crystallization, *Chem. Eng. Processing*, **31** (1992), 39-42.

[41]. Onsager, L., Electric moments of molecules in liquids, *J. Am. Chem. Soc.*, **58** (1936), No. 8, 1486-1493.

[42]. Orella, C.J., and Kirwan, D.J., The solubility of amino acids in mixtures of water and aliphatic alcohols, *Biotechnology Progress*, **5** (1989), No. 3, 89-91.

[43]. Paul, E.L., and Rosas, C.B., Challenges for chemical engineers in the pharmaceutical industry, *Chem. Eng. Prog.*, **86** (1990), No. 12, 17-25.

[44]. Randolph, A.D., and Larson, M.A., *Theory of Particulate Processes*, 2nd Ed., Academic Press, California, **1988**.

[45]. Reichardt, C., *Solvents and Solvent Effects in Organic Chemistry*, 2nd Ed., VCH, Darmstadt, Germany, **1990**.

[46]. Shanks, B.H., and Berglund, K.A., Contact nucleation from aqueous sucrose solutions, *AIChE Journal*, **31** (1985), No. 1, 152-154.

[47]. Smyth, C.P., Walls, W.S., Electric moment and molecular structure. I. The ethyl esters of mono- and dicarboxylic acids, *J. Am. Chem. Soc.*, **53** (1931), 527-539.

[48]. Stolarová, M., Buchtová, M., and Bekárek, V., Solvent polarity parameters and their mutual interrelations, *Acta Univ. palac. Olomucensis, Facultas rerum Natur. Chem. XXIII*, **79** (1984), 77-88.

[49] Street, K.W., Jr., and Acree, W.E., Jr., Estimation of the Effective Dielectric Constant of Cyclodextrin Cavities Based on the Fluorescence Properties of Pyrene-3-Carboxaldehyde, *Applied Spectroscopy*, **42** (1988), No. 7, 1315-1318.

[50]. Suppan, P., Excited-state dipole moments from absorption/fluorescence solvatochromic ratios, *Chem. Phys. Lett.*, **94** (1983), No. 3, 272-275.

[51]. Suppan, P., Local polarity of solvent mixtures in the field of electronically excited molecules and exciplexes, *J. Chem. Soc. Farad. Trans. 1*, **83** (1987), 495-509.

[52]. Suppan, P., Solvatochromic shifts: The influence of the medium on the energy of electronic states, *J. of Photochem. and Photobiology, A: Chemistry*, **50** (1990), 293-330.

[53]. Suppan, P., Solvent effects on the energy of electronic transitions: experimental observations and applications to structural problems of excited molecules, *J. Chem. Soc. A: Inorg. Phys. Theor.*, **1987**, 3125-3133.

[54]. Tavare, N.S., and Chivate, M.R., CSD Analysis from a batch dilution crystallizer, *J. Chem. Eng. Japan*, **13** (1980), No. 5, 371-379.

[55]. Uusi-Penttilä, M., and Berglund, K.A., *In situ* monitoring of antisolvent crystallization using attenuated total reflection infrared spectroscopy, Parts I and II, (manuscript).

[56]. Uusi-Penttilä, M., and Berglund, K.A., Spectroscopic Monitoring of Environmentally Benign Anti-Solvent Crystallization, *J. of Cryst. Growth*, **166** (1996), 967-970.

[57]. Uusi-Penttilä, M., Richards, R.J., Torgerson, B.A., and Berglund, K.A., Spectroscopically Determined Dielectric Constants for Various Esters, *Ind. Eng. Chem. Res.*, **36** (1997), 510-512.

[58]. Uusi-Penttilä, M., Torgerson, B.A., and Berglund, K.A., Dielectric Enrichment in Binary Systems Containing Environmentally Benign Esters, (manuscript).

[59]. Wey, J.S., Batch crystallization, In *Handbook of Industrial Crystallization*, Myerson, A.S. (Ed.), Butterworth-Heinemann, Maryland, **1993**.

MICHIGAN STATE UNIV. LIBRARIES
31293015659307